CFTR Modulates Wnt/β-Catenin Signaling and Stem Cell Proliferation in Murine Intestine

Short Title: CFTR stem cell activity and intestinal proliferation

Synopsis
This study documents the functional activity of Cftr in the active intestinal stem cell population of murine intestine. In the absence of Cftr, stem cell proliferation and Wnt/β-catenin signaling are increased, which is associated with changes in intracellular pH-dependent plasma membrane localization of Wnt-transducer Disheveled. Increased stem cell proliferation may contribute to gastrointestinal cancer risk in cystic fibrosis.

by

Ashlee M. Strubberg[1], Jinghua Liu[2], Nancy M. Walker[2], Casey D. Stefanski[1], R. John MacLeod[3], Scott T. Magness[4] and Lane L Clarke[1,2]

[1]Department of Biomedical Sciences and [2]Dalton Cardiovascular Research Center, University of Missouri, Columbia, Missouri, USA; [3]Department of Biomedical and Molecular Sciences, Queen's University, Kingston, Ontario, Canada; 4Departments of Medicine and Cell and Molecular Physiology, University of North Carolina at Chapel Hill, Chapel Hill, NC, USA

Author contributions:
AMS - Acquisition of data; analysis and interpretation of data; drafting manuscript; critical revision of manuscript
JL - Acquisition of data; analysis and interpretation of data: critical revision of manuscript
NMW - Acquisition of data; analysis and interpretation of data; statistical analysis; technical support
SDS - Acquisition of data; analysis and interpretation of data; technical support
RJM - Critical revision of the manuscript
STM – Acquisition of data; critical revision of manuscript
LLC - Study concept and design; analysis and interpretation of data; critical revision of the manuscript; obtained funding; administrative support; study supervision

The authors have no conflicts of interest.

The research was supported by a grant from the National Institute of Diabetes and Digestive and Kidney Disease (LLC: NIDDK 5R01DK048816).

Correspondent:
Lane L. Clarke, DVM, PhD
AGA Member #175531
324D Dalton Cardiovascular Research Center
University of Missouri
134 Research Park Dr.
Columbia, Missouri 65211-3300
Email: clarkel@missouri.edu
Phone: 573-882-7049

Abstract

Background & Aims: Cystic fibrosis (CF) patients and CF mouse models have increased risk for gastrointestinal tumors. CF mice exhibit augmented intestinal proliferation of unknown etiology and an altered intestinal environment. We examined the role of Cftr in Wnt/β-catenin signaling, stem cell proliferation and its functional expression in the active stem cell (ISC) population. Dysregulation of intracellular pH (pH_i) in CF ISCs was investigated for facilitation of Wnt/β-catenin signaling.

Methods: Crypt epithelia from wild-type (WT) and CF mice were compared ex vivo and in intestinal organoids for proliferation and Wnt/β-catenin signaling by standard assays. Cftr in ISCs was assessed by immunoblot of sorted $Sox9^{EGFP}$ intestinal epithelia and pH_i regulation by confocal microfluorimetry of Lgr5+-EGFP ISCs. Plasma membrane association of Wnt transducer Dvl2 was assessed by fluorescence imaging of live enteroids from WT and CF mice crossed with Dvl2-EGFP/$Rosa^{mT/mG}$ mice.

Results: Relative to WT, CF intestinal crypts showed a 25-30% increase in epithelial and Lgr5+ ISC proliferation, and increased Wnt/β-catenin signaling. Cftr was expressed in $Sox9^{EGFPLo}$ ISCs and loss of Cftr induced an alkaline pH_i in Lgr5+-EGFP ISCs. CF crypt-base columnar cells (CBCs) demonstrated a generalized increase in plasma membrane Dvl2-EGFP association as compared to WT. Dvl2-EGFP membrane association was charge- and pH-dependent, and increased in WT CBCs by Cftr inhibition.

Conclusions: Cftr KO intestine exhibits increased ISC proliferation and Wnt/β-catenin signaling. Loss of Cftr increases pH_i in ISCs and stabilizes the plasma membrane association of the Wnt transducer Dvl, likely facilitating Wnt/β-catenin signaling. Absence of Cftr-dependent suppression of ISC proliferation in the CF intestine may contribute to increased risk for intestinal tumors.

Keywords: disheveled, intracellular pH, neoplasia, stem cell

Introduction

Cystic fibrosis (CF) is a heritable genetic disease caused by mutations in the cystic fibrosis transmembrane conductance regulator gene. The gene product (CFTR) is a major anion channel of fluid transporting epithelia where it functions in transepithelial Cl^- and HCO_3^- secretion[1, 2]. CF affects multiple organs, in particular the airway epithelia where failure of mucociliary clearance results in bacterial colonization of the lung. However, intestinal disease is one of the earliest manifestations of CF and presents life-long conditions including small intestinal bacterial overgrowth (SIBO)[3], low-grade small bowel inflammation[4, 5], obstructive bowel disease[6, 7] and an increased incidence of gastrointestinal (GI) cancer[8, 9]. Cftr knockout (KO) mice recapitulate CF intestinal disease without significant manifestations of pancreatic, liver or lung disease. The disease phenotype includes a high incidence of bowel obstruction[10], low-grade bowel inflammation[11], small intestinal bacterial overgrowth[3], dysbiosis[12] and the spontaneous development of intestinal tumors with age, inclusive of invasive forms[13].

Previous in vivo studies show that Cftr KO mice exhibit increased intestinal epithelial proliferation without a corresponding increase in apoptosis[14], a condition that may predispose to intestinal neoplasia[15]. Recent epidemiological studies reveal strong correlations between the rate of stem cell division and the incidence of cancer[16]. Since the intestine has one of the highest rates of epithelial turnover in the body, pathological manifestations of CF that enhance the rate of epithelial turnover are predicted to increase the risk of gastrointestinal cancer. However, a mechanistic understanding linking the absence of Cftr activity with enhanced proliferation of the intestinal epithelium, particularly the stem cell population, has not been advanced.

Cftr is highly expressed in intestinal crypts[17, 18], the proliferative compartment of the intestine, and, by providing apical membrane Cl^- and HCO_3^- ion permeability, has an impact on the regulation of epithelial intracellular pH (pH_i). Loss of Cftr function by acute channel blockade or, chronically, in Cftr KO intestinal organoids (enteroids) results in an uncompensated alkaline pH_i in the crypt epithelium[19]. Compensation of the alkaline pH_i is impaired by a corresponding increase in intracellular Cl^- concentration $[Cl^-]_i$ which reduces cellular anion exchange activity[20]. Several aspects of cell proliferation

are known to be facilitated by an alkaline pH_i including cell cycle phase progression at G2/M[21], optimization of DNA replication[22], cytoskeleton remodeling and cell migration[23] [24], and membrane biogenesis[25]. However, cell alkalinity has also been shown to facilitate Wnt signaling[26, 27], which may directly affect stem cell proliferation.

Wnt/β-catenin signaling is essential for homeostasis and proliferation of intestinal stem cells[28] and is often aberrantly activated in intestinal cancer. In *Drosophila* spp., pH_i changes can alter Wnt signaling by modulating the interaction of the initial signal mediator Disheveled (Dvl) with the Wnt receptor Frizzled (Fz) at the plasma membrane[26]. The critical binding of Dvl's PDZ domain with the PDZ binding domain of Fz is facilitated by a stable interaction of Dvl's polybasic DEP domain to negatively charged phospholipids (phosphatidic acid, phosphatidylglycerol) at the inner leaflet of the plasma membrane. Phospholipid interaction is pH_i- and charge-dependent such that proton electrostatic interference at an acidic pH_i reduces DEP domain membrane binding and subsequent Wnt signaling[26]. We hypothesized that an alkaline pH_i in Cftr KO intestinal stem cells (ISCs) stabilizes Dvl interaction at plasma membrane thereby faciltating Wnt/β-catenin signaling.

The present study investigates augmented proliferation of the intestinal epithelium in a Cftr KO mouse model. Studies first examine whether hyperproliferation persists in Cftr KO enteroid culture, which isolates the epithelium from the immediate consequences of an abnormal Cftr KO intestinal environment (inflammation, dysbiosis) and provides the technological advantage for live crypt cell imaging[3, 11, 29]. Second, studies evaluate the activation status of Wnt/β-catenin signaling in the Cftr KO intestine and the functional activity of Cftr in ISCs, specifically, Lgr5+ stem cells[30]. Third, live cell imaging is used to examine the hypothesis that alkalinity of Cftr KO intestinal crypt-base columnar stem cells is conducive to increased interaction of Dvl (i.e., the major isoform Dvl2[31]) with the plasma membrane for Wnt signaling.

Materials and Methods

Mice. Mice with gene targeted disruptions of the murine homolog of *Cftr* [*abcc7*, Cftr knock-out (KO)] and sex-matched wild-type (WT, +/+ or +/-) littermates were used[10].

Mice were outbred to Black Swiss (Charles River) at generational intervals and resultant F1 heterozygotes were crossed to generate F2 offspring for experimentation. The Cftr KO mouse line was crossed with Lgr5-EGFP-IRES-creERT2 (Lgr5-EGFP) mice, to generate WT/Lgr5-EGFP and Cftr KO/Lgr5-EGFP mice. The Cftr KO mouse line was also crossed with both Dvl2 KO/Dvl2-EGFP BAC transgenic[32] and Gt(ROSA)$^{26Sortm4(ACTB-tdTomato,-EGFP)Luo}$/J (Rosa$^{mT/mG}$, Jackson Labs) mouse lines to generate WT and Cftr KO/Dvl2 KO/Dvl2-EGFP/Rosa$^{mT/mG}$ expressing mice. Genotypes were identified by PCR analysis of tail-snip DNA as previously described for mutant Cftr[33], Dvl2 KO and Dvl2-EGFP expression[34], and Rosa$^{mT/mG}$ (Jackson Labs). Copy number for the Dvl2-EGFP transgene was verified by TaqMan® GFP copy number assay (Applied Biosystems). Only mice expressing 2 copies of the Dvl2-EGFP transgene were used for experimental analysis. All mice were maintained *ad libitum* on standard laboratory chow (Formulab 5008, Rodent Chow; Ralston Purina) and distilled water containing Colyte® (Schwartz Pharma) laxative to prevent intestinal obstruction in the Cftr KO mice. Mice were housed individually in a temperature- and light-controlled room (22-26°C; 12-hour light: 12-hour dark cycle) in the Association for Assessment and Accreditation of Laboratory Animal Care- accredited animal facility at the Dalton Cardiovascular Research Center, University of Missouri. All experiments involving animals were approved by the University of Missouri IACUC.

Enteroid culture. The enteroid culture has been previously described in detail[19]. Cultures were overlaid with growth medium containing Ham's F-12 medium with 5% FBS, 50 µg/mL gentamicin, 125 ng/mL R-spondin1, 25 ng/mL noggin and 12.5 ng/mL epidermal growth factor. Growth medium was changed every 3-4 days and enteroids were passaged every 7-10 days using Cell Recovery Solution (BD Sciences). Passages 1-2 were used for experimentation.

Lgr5-EGFP cell counts. Crypts were isolated from WT/Lgr5-EGFP or Cftr KO/Lgr5-EGFP mice and fixed immediately in 10% buffered formalin (Sigma-Aldrich), or cultured as enteroids in growth medium before fixation. Z-stack images were acquired using either a TCS SP5 Confocal-Multiphoton microscope built on a DMI6000 inverted platform (Leica, Wetzler, Germany) or an Olympus Fluoview confocal microscope

(FV1000). Images were reconstructed in 3D using Imaris® Software (version 7.7.1, Bitplane, Concord, MA) and the number of Lgr5-EGFP positive stem cells identified in three-dimensions was counted for each crypt.

Immunofluorescence. Freshly isolated crypts or enteroids were fixed in 10% buffered formalin (Sigma-Aldrich) or 4% paraformaldehyde and stored at 4°C until processing. Fixed enteroids and Matrigel™ were scraped from the culture dishes, transferred to 1.5mL tubes, centrifuged at 200*g* (1min) and washed 3x with 1X PBS to remove Matrigel™ and fixative. Samples were permeabilized for 60mins using 0.5% Triton X-100 (Sigma-Aldrich) in PBS and blocked for 30min with gentle shaking in fish skin gelatin buffer [10mM Tris, 5mM EDTA, 0.15M NaCl, 0.25% fish skin gelatin (Sigma-Aldrich), 0.05% Tween20]. Samples were incubated overnight at 4°C with primary antibody diluted in fish skin gelatin buffer, washed 3x in fish skin gelatin buffer, and incubated with secondary antibody for 4-5 hours with gentle shaking at 4°C. After removal of the secondary antibody, samples were washed three times for 10mins in fish skin gelatin buffer. Samples were then resuspended in SlowFade® gold antifade mounting medium (Thermo Fisher Scientific) and sealed under glass coverslips on microscope slides (Fisher Scientific). Fresh crypts and enteroids were imaged using an Olympus Fluoview confocal microscope. Z-stacks were imaged to determine crypt cross-sections post-acquisition using Imaris® software. Anti-Frizzled 7 (10 µg/mL, R&D Systems, AF198) was used as primary antibody and secondary antibody was anti-goat IgG Alexa Fluor® 405 (Abcam, ab175665) used at a 1:500 dilution in fish skin gelatin buffer.

Proliferation assays: Proliferation of WT and Cftr KO freshly isolated crypts was measured by immunofluorescence for mitotic cells using anti-Phospho-Histone H3 (PH3) primary antibody (1:100 dilution, Millipore, 06-570) in fish skin gelatin buffer (see methods above). Nuclei were labeled with TO-PRO 3 (Thermo Fisher Scientific) nuclear stain (1:2000 dilution in PBS) in fish skin gelatin buffer. Proliferation of enteroid crypts (p1 or p2, 5-7 days) maintained in growth medium was measured using the Click-iT 5-ethynyl-2'-deoxyuridine (EdU) assay to label cells in S phase of the cell cycle, according to the manufacturer's protocol (Thermo Fisher Scientific) and as previously

described[35]. Enteroids were exposed in situ to EdU for 15mins and fixed in 4% paraformaldehyde (PFA) and stored at 4°C. Fixed enteroids and Matrigel™ were scraped from the culture dishes, transferred into 1.5mL tubes, and centrifuged at 200*g* for 1min. The supernatant containing Matrigel™ was aspirated and the fixed enteroids were washed twice with 1X PBS. Nuclei were labeled with Hoechst 33342 diluted 1:2,000 for 1 h. Labeled enteroids were concentrated by brief centrifugation (200*g*, 1min), resuspended in SlowFade® gold antifade mounting medium (Thermo Fisher Scientific) and sealed under a glass coverslip on microscope slides. Crypts were imaged on an Olympus Fluoview confocal microscope. Post-acquisition 3D reconstructed Z-stacks (Imaris® Software, Bitplane) were used to determine crypt cross sections for counting of PH3-positive (PH3+), EdU-positive (EdU+) and total nuclei. Acquired images were coded and nuclei counting was performed by an observer blinded to genotype.

Immunoblot analysis. Freshly isolated crypts, enteroids or sorted intestinal epithelial cells were suspended in ice-cold RIPA buffer (Cell Signaling) containing HALT Protease inhibitor (Thermo Fisher Scientific) and lysed at 4°C by supersonication. Total lysate protein was loaded on 10% SDS-PAGE gels for electrophoresis, membrane transfer and immunoblotting. Anti-active β-catenin (1:2000 dilution, Millipore, 05-665), anti-Lef1 (1:500 dilution, Santa Cruz, sc-28687) and anti-Cftr 3G11 (1:2000 dilution, provided by CFTR Folding Consortium, Cystic Fibrosis Foundation Therapeutics) were used as primary antibodies. Anti-β-actin (1:2000 dilution, Santa Cruz, sc-130656) or anti-GAPDH (1:2000 dilution, Santa Cruz, sc-25778) were used as loading controls. Densitometry was performed using Image Lab™ Software (version 5.2.1, BioRad).

Quantitative RT-PCR array. Enteroids were removed from Matrigel and processed for total RNA extraction as previously described[19]. cDNA was mixed with TaqMan Gene Expression Master Mix (Applied Biosystems), according to the manufacturer's protocol, and loaded onto customized 96-well mini-array plates containing TaqMan assays for the genes of interest. β-actin served as the manufacturing control, and three housekeeping genes (β-glucuronidase (Gusb), hypoxanthine guanine phosphoribosyl transferase 1 (Hprt1), and mitochondrial ribosomal protein L19 (Mrpl19)) were also assayed. A

Mastercycler EP RealPlex thermocycler (Eppendorf, Hamburg, Germany) was used for quantitative PCR. The threshold cycle (C_t) of a gene of interest was subtracted from the geometric mean C_t of the housekeeping genes to yield ΔC_t. The relative mRNA expression of Cftr KO vs. WT was calculated using the $\Delta\Delta C_t$ method[36].

FACS. Isolated small intestinal crypt cells from $Sox9^{EGFP}$ mice were dissociated for fluorescence-activated cell sorting, as previously described[37]. Sox9EGFPNegative, Sox9EGFPSublo, Sox9EGFPLo and Sox9EGFPHigh cell were isolated using a MoFlo FACS machine (Dako,/Cytomation). Cell were collected in radioimmunoprecipitation assay (RIPA) buffer and frozen at -20°C for protein immunoblotting.

Confocal microfluorimetry of intracellular pH. WT, Cftr KO, WT/Lgr5-EGFP and Cftr KO/Lgr5-EGFP enteroids were cultured in growth medium for 5-7 days on glass-bottomed Fluorodishes (World Precision Instruments). Enteroids were loaded with the ratiometric pH sensitive dye SNARF-5F (Thermo Fisher Scientific) at 40μM for 30min at 37°C as previously described[19]. For basal conditions, cultures were continuously superfused with Kreb's bicarbonate Ringer (KBR) + 5mM N-tris(hydroxymethyl)-methyl-2-aminoethanesulfonic acid (TES) buffer and gassed with 95% O_2: 5% CO_2 (pH 7.4, 37°C). For Cftr KO enteroids grown in pH 7.1 or 6.6 medium, enteroids were imaged in static culture medium (pH 7.1 or 6.6) with an overlying 95% Air: 5% CO2 atmosphere maintained at 37°C using a culture dish incubator DH-35iL (Warner Instruments, 64-0349).. All images were acquired with a TCS SP5 Leica Confocal microscope in a temperature controlled incubator. The excitation source for SNARF-5F was a 514 nm argon laser and images were collected at dual emission wavelengths (580 ± 30 and 640 ± 30 nm). Z-stacks of individual crypts were imaged and regions of interest (ROI) were placed post-acquisition using Imaris® Software. For intracellular regional pH_i studies, ROI were placed on cross-sectional slices at the basal or apical aspect of CBCs near the +4 position (to avoid Paneth cell granule fluorescence) using SlideBook 5.0 (Intelligent Imaging Innovations, Denver, CO). The 580-to-640-nm ratio was converted to pH_i using a standard curve generated by the K^+/nigericin technique in unlabeled and Lgr5-EGFP-positive cells[38].

Live imaging of enteroids for Dvl2-EGFP membrane association. Passaged enteroids were plated in Matrigel® onto Fluorodishes (World Precision Instruments) and cultured for 5-7 days prior to imaging. Unless indicated otherwise, enteroids were gassed with 95% air: 5% CO_2 and maintained at 37°C using a culture dish incubator DH-35iL (Warner Instruments, 64-0349) during all acquisitions. Z-stacks were acquired using an Olympus Fluoview confocal microscope (FV1000). Dvl2-EGFP proximity to the plasma membrane of CBCs in live enteroid crypt was assessed post-acquisition in crypt cross-sectional slices selected from 3D reconstructed images using Imaris® Software. CBCs were selected based on 1) location at cell positions 1-3; 2) lack of granulation as defined by the absence of a granule theca outlined by $Rosa^{mT/mG}$ label (prominent in Paneth or goblet cells); 3) a contiguous and well-defined $Rosa^{mT/mG}$ labeled plasma membrane; and 4) not overtly undergoing cell division as indicated by a nuclear position apical to the basal membrane and membrane accumulation at the apical pole of the cell. Using ImageJ software (version 1.49, Bethesda, MD), preliminary studies indicated that Dvl2-EGFP intensity measurements taken at CBC plasma membrane adjacent to the nucleus were confounded technically (due to minimal cytoplasm and curvature of the nucleus) and conceptually (apposition of nuclear and plasma membranes). Therefore, measurement of the juxtamembrane Dvl2-EGF intensity was confined to the supranuclear portion of CBCs, i.e., apical to the nucleus. Acquired images were coded and measurement of juxtamembrane Dvl2-EGFP was performed by an observer blinded to genotype. To quantitate membrane proximity of Dvl2-EGFP at the supranuclear plasma membrane of CBC, the $Rosa^{mT/mG}$ labeled plasma membrane was outlined as a ROI using red fluorescent images of cell cross-sections using ImageJ software. The ROI was transferred to the EGFP image of the CBC for measurement of Dvl2-EGFP intensity within a two-pixel distance (1.15 μm) interior to the supranuclear plasma membrane, except at the apical (brush border) membrane. The leading and trailing plasma membrane, defined as distal and proximal to cell position 0 respectively were individually analyzed for juxtamembrane Dvl2-EGFP intensity along the length of the supranuclear region.. Crypt position 0 was often occupied by visible Paneth cells in the chosen slice. The average Dvl2-EGFP intensity of pixels was also acquired for the entire supranuclear region of each CBC. Differences in EGFP intensity between CBCs

were normalized as the ratio of average juxtamembrane EGFP intensity at the leading or trailing plasma membrane ÷ average EGFP intensity of all pixels in the supranuclear region of the CBC. Average EGFP intensity of pixels in the supranuclear region were not significantly different between WT and Cftr KO CBCs (Ave. intensity = 59.5±8.8 for WT and 88.5±15.9 for Cftr KO, ns, n = 7-6, respectively.

Charge- and pH_i-dependence of Dvl2-EGFP association with the plasma membrane in Cftr KO enteroids. Cftr KO enteroids were treated with either sphingosine (Avanti Polar Lipids), low bicarbonate medium or bumetanide (50 μM) plus carbachol (100 μM CCH), to alter Dvl2-EGFP localization at the plasma membrane. For experiments using sphingosine to neutralize negative charges at the inner leaflet of the plasma membrane, Cftr KO enteroids were treated at 75μM in growth medium for 1hr prior to imaging (95% ethanol: 5% water used as vehicle, 1:2000 final dilution). After 3 days culture in standard medium, Cftr KO enteroids were acidified by 2 days culture in low bicarbonate (3.6mM bicarbonate, 7mM Sodium TES, 6.8mM Mannitol, pH 6.6) medium and compared to Cftr KO enteroids maintained in standard medium (14mM bicarbonate, pH 7.1). Acute reduction in intracellular Cl^- and pH_i in Cftr KO enteroids was achieved by co-treatment of bumetanide (50μM, Sigma; dissolved in 95% ETOH) and CCH (100μM, Sigma), as previously described[20]. Briefly, Cftr KO enteroids were treated with bumetanide for 15mins to block Cl^- uptake by the basolateral $Na^+/K^+/2Cl^-$ cotransporter Nkcc1 followed by co-treatment with CCH for 15 mins to activate Cl^- efflux via Ca^{2+}-activate Cl^- channels (e.g., Ano1). The treatment lowers intracellular Cl^- concentration sufficiently to facilitate activity of the basolateral anion exchanger 2 (Ae2). To acutely block Cftr, WT enteroids were treated with a combination of $Cftr_{inh}$-172 (10 μM, Sigma) and GlyH101 (20 μM, Sigma) dissolved in DMSO for 1 hr. to evaluate changes in Dvl2-EGFP association with the plasma membrane. Measurements of Dvl2-EGFP intensity were performed as above by an observer blinded to treatment.

Materials. EGF, noggin and Wnt3a were obtained from R&D Systems (Minneapolis, MN). Recombinant Rspondin1 was isolated as described previously[39].

Statistics. Cumulative data are reported as the mean ± SE. Intracellular pH data are the average of individual Lgr5-EGFP or crypt-base columnar cells in crypts from Individual

mouse averages are shown for juxtamembrane EGFP intensity which are derived from the average of 1-3 crypt-base columnar cells/crypt from 2-4 crypts of both passage 1 and 2 enteroids. Intracellular pH is the average of Lgr5-EGFP or crypt base columnar cell from rSignificant differences between female and male mice were not found for baseline membrane localization of Dvl-EGFP or pH_i of Lgr5-EGFP/crypt-base columnar-cells, so these data were combined in the averages. Data between two groups were compared using a two-tailed Student *t*-test or, if not normally distributed with equal variances, by Mann-Whitney Rank Sum test. $\Delta\Delta C_t$ data were analyzed using a one-sample *t*-test with test mean=0. A probability value of $P < 0.05$ was considered statistically significant.

Results

Increased intestinal proliferation in Cftr KO intestinal crypts is recapitulated in early passage enteroids. Previous in vivo studies of the Cftr KO mouse intestine demonstrated a 34% increase in epithelial proliferation measured by proliferating cell nuclear antigen labeling without a change in apoptosis as compared to WT intestine[14]. To assess intestinal hyperproliferation in our Cftr KO mice in vivo, mitotic cells identified as anti-Phospho Histone H3-positive (PH3+) cells, were enumerated by confocal microscopy using freshly isolated crypts from the proximal small intestine of Cftr KO and WT sex-matched littermates (Fig. 1A). Cftr KO crypts had a 36% increase in the percentage of PH3+ (%PH3+) cells per crypt optical cross-section. Mitotic figures were found in both crypt base (< +4 cell position) and the transit-amplifying zone (> +4 position), of each genotype, indicating proliferation in the ISC and progenitor cell populations. Crypt base columnar cells represent the active ISC population and express the ISC marker Leucine-rich G-protein coupled Receptor 5 (Lgr5)[40]; therefore, Cftr KO heterozygous mice were crossbred with Lgr5-EGFP-ires-CreERT2 (Lgr5-EGFP) mice to compare proliferation in the active Lgr5+ stem cell population[30]. Using freshly isolated crypts from sex-matched WT/Lgr-5-EGFP and Cftr KO/Lgr-5-EGFP littermate mice, the number of Lgr5-EGFP-labeled cells was enumerated for each crypt containing at least one Lgr5-EGFP+ cell. As shown in Fig. 1B, the average number of Lgr5-

EGFP+ cells per crypt was significantly greater in the Cftr KO/Lgr5-EGFP intestine as compared to WT/Lgr5-EGFP intestine (30.4% increase in mean Lgr5-EGFP+/crypt).

Murine enteroids are well-differentiated, primary cultures of the small intestinal epithelium that can undergo multiple passages[30]. Enteroid crypts express functional Cftr activity in WT enteroids proliferating at rates that recapitulate in vivo rates by reduced (20%) growth factor supplementation , as used in the present study[19].

Figure 1

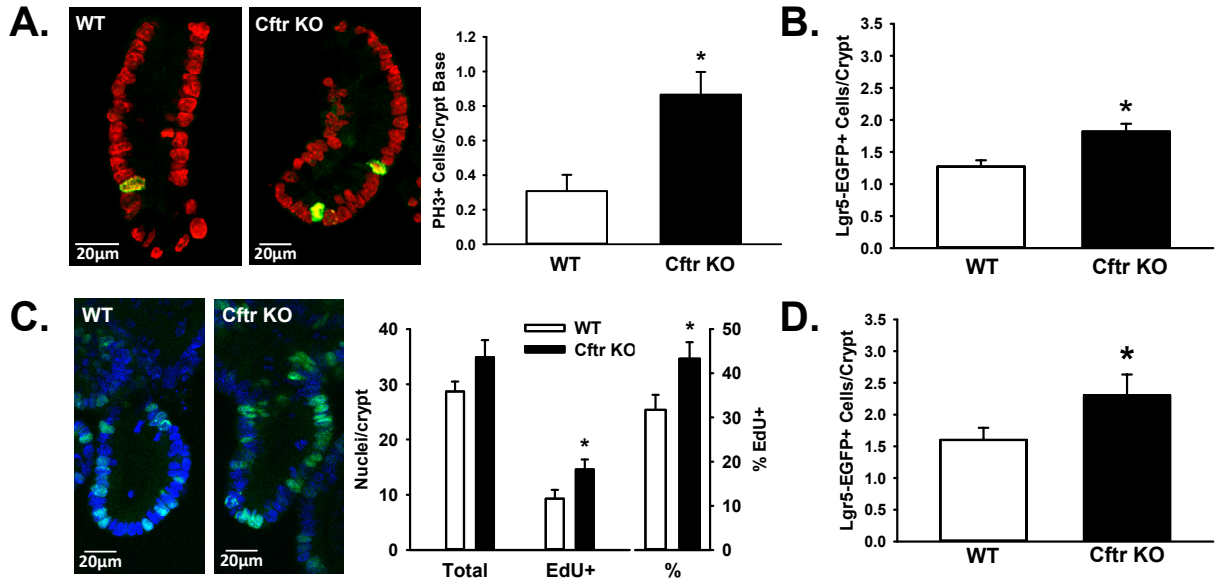

Fig. 1. *Increased proliferation in the Cftr KO intestine in vivo and early passage enteriods.* *A*: Left, isolated crypts from WT and Cftr KO mice labeled for phospho-Histone H3 (PH3) (green), a marker of mitosis. Nuclei are labeled with TO-PRO 3 nuclear stain (red). Magnification, 600X. Right, cumulative data showing differences in proliferation between freshly-isolated WT and Cftr KO crypts as measured by PH3 immunofluorescence. Data is expressed as percent PH3+ (%PH3+) cells/total nuclei per crypt optical cross-section; n=4 WT/Cftr KO pairs (32-38 crypts/genotype) *P<0.001. *B*: Cumulative data showing the average Lgr5-EGFP+ stem cell numbers/Lgr-EGFP+ crypt in freshly-isolated crypts from WT/Lgr5-EGFP and Cftr KO/Lgr5-EGFP small intestine. Cumulative data showing distribution of Lgr5-EGFP positive cells/crypt. *P<0.02; n= 3 WT/Cftr KO pairs (81-113 Lgr5+ crypts/genotype). *C*: Left, enteroid crypts from WT and Cftr KO mice labeled with EdU for S phase nuclei (green). Nuclei are labeled with DAPI nuclear stain (blue). Magnification, 600X. Right, cumulative data showing differences in proliferation between WT and Cftr KO enteroid crypts as measured by EdU-positive (EdU+) nuclei and the percentage of EdU+ (%EdU+ nuclei) per crypt optical cross-section. n=5 WT/Cftr KO pairs (52-48 crypts/genotype). *P<0.03. *D*. Cumulative data showing the average Lgr5-EGFP+ stem cell numbers/Lgr-EGFP+

crypt in enteroid crypts from WT and Cftr KO small intestine. *P<0.05, n = 5 WT/Cftr KO pairs (156-171 Lgr5+crypts/genotype).

Enteroids from WT and Cftr KO mice enable imaging of live cellular processes in real-time. Furthermore, enteroids avoid the immediate consequences of the abnormal CF intestinal environment[11,3,12,10] which includes inflammatory mediators and reparative processes that can alter Wnt/β-catenin signaling and ISC proliferation[41,42]. Using passage 1 and 2 cultures, WT and Cftr KO enteroids were exposed to 5-ethynyl-2'-deoxyuridine (EdU) to enumerate cells in S phase. As shown in Fig. 1C, EdU incorporation revealed a 37% increase in proliferation of Cftr KO enteroid crypts compared to WT, as assessed by increases in the total number of EdU+ cells and %EdU+ cells per crypt cross-section in the Cftr KO enteroid crypts. To estimate ISC proliferation, the number of Lgr5-EGFP+ cells in crypts containing at least one Lgr5-EGFP+ cell were enumerated in passage 1 and 2 enteroids from sex-matched WT/Lgr-5-EGFP and Cftr KO/Lgr-5-EGFP littermate mice. As shown in Fig. 1D, Lgr5-EGFP+ cells/crypt were significantly greater in the Cftr KO/Lgr5-EGFP as compared to WT/Lgr5-EGFP enteroids (44% increase in mean Lgr5-EGFP/crypt).

We next asked whether later passages (i.e., passage 4) of Cftr KO enteroids would maintain high rates of proliferation, thereby suggestive of an epithelial-autonomous effect of Cftr ablation. At passage 4, WT and Cftr KO enteroids showed similar proliferation rates as measured by EdU labeling. However, the change was largely due to increased proliferation in the WT enteroid crypts which changed from 31.7±3.4 %EdU+ of total crypt nuclei in early passages to 42.8±3.5% EdU+ at passage 4 ($p<0.002$, n=5-6). Cftr KO enteroids averaged 42.3±3.7% EdU+ of total crypt nuclei in early passage and 42.5±2.2% EdU+ at passage 4 (ns, n=5). Corresponding to the increased proliferation in the WT at passage 4, immunoblot analysis of passage 4 WT enteroids revealed decreased protein expression of Cftr (-50.6% relative to passage 1, $P<0.022$, n = 4-6 WT mice). These findings are consistent with earlier studies of cell lines expressing human CFTR, which showed suppression of CFTR expression and down regulated proliferation as compared to cells expressing dysfunctional CFTR[43, 44]. Cells with low levels of CFTR activity have a growth advantage and dominate in subsequent generations, which apparently extends to subsequent passages of WT enteroid cultures.

Increased Wnt/β-catenin signaling in Cftr KO intestinal crypts is recapitulated in early passage enteroids. Wnt/β-catenin signaling is required for the maintenance of the ISC population[28]. With evidence of increased proliferation in both freshly-isolated Cftr KO crypts and Cftr KO enteroids, we asked whether Wnt/β-catenin signaling contributed to increased proliferation in the Cftr KO intestine. Freshly-isolated crypts and enteroids from the same sex-matched WT and Cftr KO littermates were compared by immunoblot analysis for levels of active β-catenin, defined as β-catenin dephosphorylated at Ser37 and Thr41[45], and an immediate down-stream Wnt target gene, Lef1[46]. As a positive control for enhanced Wnt/β-catenin signaling, WT enteroids were also treated with Wnt-conditioned medium for 24 hrs. before collection. The immunoblot shown in Fig. 2A indicates that that both freshly-isolated crypts and the derived enteroids from Cftr KO mice have greater levels of active β-catenin and Lef1 as compared to those from their WT littermates, and similar to Wnt-treated WT enteroids. Densitometric analysis showed statically significant increases in active β-catenin and Lef1 in fresh crypts (Fig. 2B) and in the derived enteroids (Fig. 2C). Notch1 signaling can act cooperatively with the Wnt signaling pathway[47, 48]. Activation of Notch1 signaling was assessed by immunoblots of freshly-isolated crypts for the Notch intracellular domain (NICD), which serves as a co-transcription factor in the regulation of ISC proliferation[48]. However, there was no significant difference in Notch1 pathway activation between Cftr KO and WT crypts (relative to WT (100%): 106±20%, ns, n=6 WT-Cftr KO sex-matched littermate pairs. The above findings indicate that increased Wnt/β-catenin signaling contributes to increased ISC proliferation in Cftr KO intestine in vivo and in early passage enteroids.

Cftr expression and function in WT Lgr5+ intestinal stem cells. CFTR possesses an intestinal-specific enhancer element in intron 1 that is positively regulated by Tcf4 and therefore a target for Wnt signaling[49]. Based on finding increased Lgr5-EGFP+ stem cell proliferation in the Cftr KO intestine (Fig. 1) and evidence that CFTR functions as a growth suppressant/tumor suppressor[13, 43, 44], we asked whether Cftr activity is present in ISCs. Different expression levels of SOX9 transcription factor modulate intestinal stem cell proliferation and serve as a marker of crypt cell type[37]. Fluorescence-

Figure 2

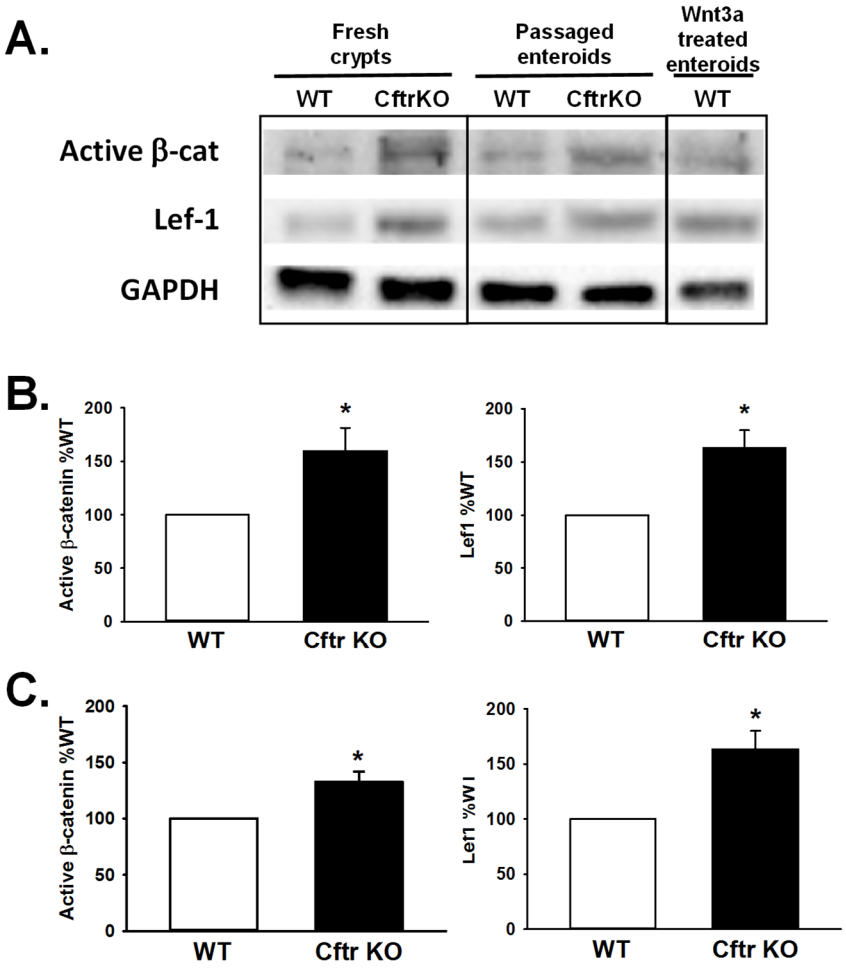

Fig. 2. *Increased Wnt/β-catenin signaling in the Cftr KO intestine in vivo and early passage enteroids.* *A*: Immunoblot for active β-catenin (de-phosphorylated at Ser37/Thr41) and down-stream Wnt target gene Lef1 using freshly-isolated crypts (Fresh Crypts) and passage 1 enteriods (Passaged Enteroids) from a sex-matched, littermate pair of WT and Cftr KO mice Far right panel, WT enteroids treated with Wnt-conditioned medium for 24 hrs. before collection. *B*. Left, densitometric analysis for immunoblots of active β-catenin from WT and Cftr KO freshly-isolated crypts. GAPDH or β-actin used as loading controls. Data represented as % WT; n=11 WT/Cftr KO pairs. **P*<0.03. Right, densitometric analysis for immunoblots of Lef1 protein expression from WT and Cftr KO isolated crypts. GAPDH used as loading control. Data represented as % WT; n=7 WT/Cftr KO pairs. *C*: Left, densitometric analysis for immunoblots of active β-catenin from sex-matched littermate WT and Cftr KO enteroids. GAPDH used as loading controls. Data represented as % WT; n=5 WT/Cftr KO pairs. **P*<0.02. Right, densitometric analysis for immunoblots of Lef1 protein expression in WT and Cftr KO enteroids. GAPDH used as loading control. Data represented as % WT; n=4 WT/Cftr KO pairs. **P*<0.03.

activated cell sorting of intestinal epithelium from $Sox9^{EGFP}$ transgenic mice have shown that low-expressing $Sox9^{EGFP}$ ($Sox9^{EGFPLo}$) cells are CBCs that are enriched in Lgr5 and form enteroids in culture[37, 50]. Therefore, intestinal epithelial cells from $Sox9^{EGFP}$ mice were sorted into expression fractions and immunoblotted for Cftr. As shown by the immunoblot in Fig. 3A, the $Sox9^{EGFPLo}$ cell fraction had a significant amount of Cftr relative to the $Sox9^{EGFPSubLo}$ fraction, representing transit-amplifying progenitor cells, and the $Sox9^{EGFPNeg}$ fraction, representing the differentiated cell types including enterocytes, goblet cells and Paneth cells. An analysis of Cftr expression in WT small intestinal epithelial cells that were sorted to include the fraction showing high expression of $Sox9^{EGFP}$ representing enteroendocrine cells and +4 ISCs is shown in Supplemental Fig. 1. To investigate Cftr functional activity in ISCs, we examined the effect of Cftr loss on the intracellular pH (pH_i) of Lgr5-EGFP+ stem cells in the crypt-base of enteroids from sex-matched littermate WT/Lgr-5-EGFP and CftrKO/Lgr-5-EGFP mice. Previous studies have shown that acute inhibition of Cftr using the channel blocker $Cftr_{inh}$-172 (1 hr.) alkalizes pH_i in the crypt epithelium of WT enteroids[19]. More importantly, pH_i of crypt epithelium in Cftr KO enteroids is uncompensated and maintains an alkaline pH_i[19, 20], similar to reports of duodenal villous epithelium from Cftr KO mice[38, 51] and CFPAC cells, a pancreatic cell line derived from a CF patient[52]. To measure intracellular pH in crypt-base Lgr5-EGFP+ stem cells (Fig. 3B), enteroids were loaded with the ratiometric, pH-sensitive dye SNARF 5F for confocal microfluorimetry. As shown in Fig. 3C, the pH_i in WT Lgr5-EGFP stem cells significantly increased by ~0.2 pH units following a 1 hr. treatment with the Cftr channel blocker $Cftr_{inh}$-172 (10 mM). Moreover, as shown in Fig. 3D, Cftr KO Lgr5-EGFP+ stem cells exhibit an alkaline pH_i that is also ~0.2 pH units greater than in WT Lgr5-EGFP+ stem cells. These findings indicate that both acute and chronic loss of Cftr modulates pH_i into the alkaline range of Lgr5-EGFP+ intestinal stem cells, indicative of a pH_i regulatory role by Cftr anion channel activity in WT ISCs.

Primary culture of dissociated small intestinal crypt epithelium with exogenous Wnt3a (100 ng/mL) results in the formation of ISC–enriched epithelial spheroids (enterospheres)[53-57]. In examining Cftr stem cell activity, we asked whether ISC-enriched enterospheres from WT and Cftr KO would exhibit differences in proliferation consistent with the study enumerating Lgr5-EGFP+ ISCs (Figs 1B, 1D). As shown in

Figure 3

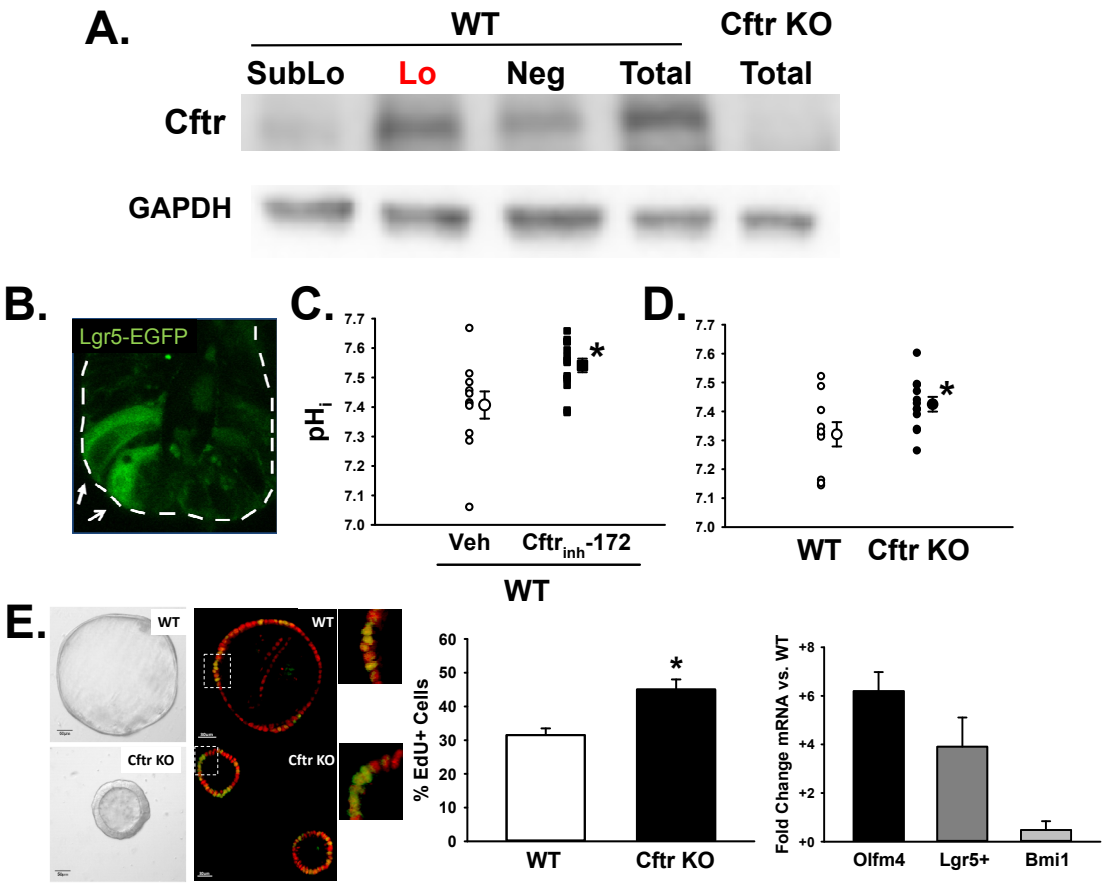

Fig. 3. *Expression and function of Cftr in the active population of small intestinal stem cells.* *A*. Immunoblot for Cftr in flow cytometry cell fractions of small intestinal epithelium isolated from Sox9^{EGFP} mice. Sublo, sub-low Sox9^{EGFP}-expressing cell fraction (transit-amplifying progenitors); Lo, low Sox9^{EGFP}-expressing cell fraction (crypt-base stem cells, Lgr5+); Neg, negative for Sox9^{EGFP} expression cell fraction (enterocyte, goblet, Paneth); Total, total small intestinal epithelium. Cftr KO total epithelium, negative control. GAPDH, loading control. Representative of 3 Sox9^{EGFP} and Cftr KO mice. *B*. Confocal micrograph showing Lgr5-EGFP-expressing intestinal stem cells in crypt epithelium (white arrows). White dashed line, outline of crypt. *C*. Intracellular pH of Lgr5-EGFP+ cells in WT/Lgr-5-EGFP enteroids treated with either DMSO (Veh, small circles) or Cftr$_{inh}$-172 (10 μM for 1 hr, small squares). Treatment average shown as large black circle or square. * $p < 0.02$ vs. Veh, n = 10-13 Lgr5-EGFP cells from 7-8 enteroids cultured from 6 WT/Lgr-5-EGFP mice. *D*. Intracellular pH of Lgr5-EGFP+ cells in enteroids from sex-matched WT/Lgr-5-EGFP (open small circles) and Cftr KO/Lgr-5-EGFP (black small circles) littermate mice. Average shown as large circles. *$p<0.04$, n = 10-12 Lgr5-EGFP cells from 6 enteroids from 3 sex-matched WT/Lgr-5-

EGFP and Cftr KO/Lgr-5-EGFP littermate mice. *E*. Left, ISC-enriched enterospheres from sex-matched WT and Cftr KO littermate mice. Also shown are EdU positive nuclei (green) and nuclei (red) in an optical cross-section of enterospheres from WT and Cftr KO mice. Middle, percentage of EdU-positive nuclei relative to total nuclei in optical cross-sections of WT and Cftr KO enterospheres. Average number of nuclei/enterosphere were WT = 36.1±3.8; Cftr KO = 46.7±2.0, n = 32 enterospheres/genotype; $p<0.009$). *$p<0.05$ vs. WT. n= 4 sex-matched WT and Cftr KO littermate mice (8 enterospheres/mouse). Left, fold change in mRNA expression of stem cell markers in in Cftr KO enterospheres relative to WT, n =3 sex-matched WT and Cftr KO littermate mice.

Fig. 3E (left), WT enterospheres formed enlarging monolayer cysts, suggesting Cftr-mediated fluid secretion. In contrast, Cftr KO enterospheres had much smaller luminal cavities and expanded slowly with time in culture, as noted previously in studies of human CF colon organoids[58]. EdU and confocal optical cross-section studies were used to examine proliferation in WT and Cftr KO enterospheres. As shown in Fig. 3E (middle), Cftr KO enterospheres had a 43% greater rate of proliferation relative to WT enterospheres. Moreover, qRT-PCR revealed higher mRNA expression of stem cell markers (Olfm, Lgr5, Bmi1)[40, 59, 60] in the Cftr KO enterospheres versus WT (Fig. 3E, right). These findings demonstrate a role of Cftr as growth suppressant in an enriched ISC population.

Increased intracellular alkalinity and membrane association of Dvl2-EGFP in Cftr KO crypt-base columnar cells. Different facets of Wnt signaling play major roles in cellular processes of proliferation, cell migration and polarity[27]. The signaling mediator Disheveled (Dvl) is critical for downstream activation of both canonical and non-canonical Wnt signaling pathways through its recruitment to Frizzled (Fz) membrane receptors[61]. The formation of a stable Dvl-Fz association involves both the binding of the PDZ domain of Dvl to the PDZ binding domain of Fz and the binding of the polybasic DEP domain of Dvl to negatively charged phosphatidic acid (PA) and phosphatidylglycerol (PG) at the inner leaflet of the plasma membrane[26,62]. The latter process is both charge- and pH_i-dependent, wherein a more alkaline pH_i facilitates electrostatic attraction of the polybasic DEP domain to the cell membrane. Importantly, the three major domains of Dvl are conserved across species, including the PDZ and DEP domains[27]. Based on evidence of alkalinity and increased proliferation in Cftr KO ISCs, we asked whether Dvl in Cftr KO CBCs associates more closely with the plasma membrane as a means to facilitate Wnt/β-catenin signaling.

Subcellular localization of the major Dvl isoform in mice, Dvl2, was imaged in cultured WT and Cftr KO enteroids from transgenic mice that express Dvl2-EGFP (native Dvl2 KO) and the $Rosa^{mT/mG}$ plasma membrane reporter (Fig. 4A). Enteroids from WT/Dvl2-EGFP/$Rosa^{mT/mG}$ and Cftr KO/Dvl2-EGFP/$Rosa^{mT/mG}$ mice were cultured in growth medium and CBCs were imaged in situ using confocal fluorescence microscopy.

Figure 4

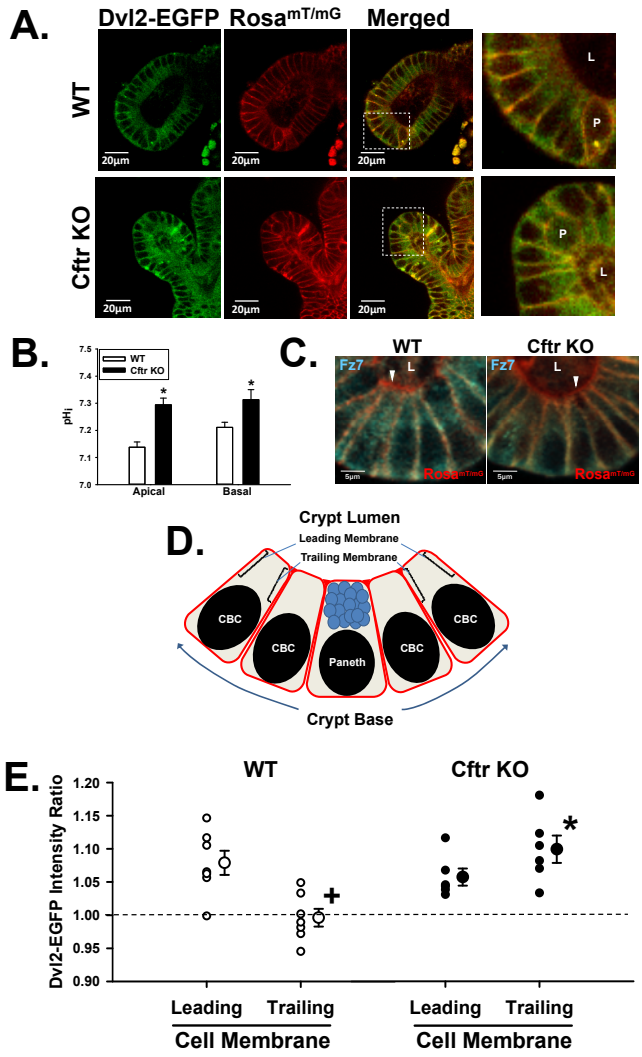

se

Fig. 4. *Increased Dvl2-EGFP localization at the plasma membrane in Cftr KO crypt-base columnar cells. A.* Representative images of WT/Dvl2-EGFP/Rosa$^{mT/mG}$ (top) and Cftr KO/Dvl2-EGFP/Rosa$^{mT/mG}$ (*bottom*) enteroid crypts. *Far right*, 3.6X enlargement of merged images of CBCs (from white boxes). P, Paneth cell; L, crypt lumen. Magnification, 600X. *B.* Cumulative pH_i data for the apical and basal regions of crypt-base columnar cells (CBCs) in crypts of WT and Cftr KO enteroids. *p<0.05 vs. WT; n = 4-8 crypts from 3 sex-matched WT and Cftr KO littermate mice. *C.* Immunofluorescence image of Frizzled 7 (Fz7, blue) plasma membrane (red) expression of CBCs in WT and Cftr KO enteroid crypts. Shown are 2.3X enlargement of merged images. Representative of 3 WT-Cftr KO mouse pairs. L, lumen. White arrowheads denote lack of Fz7 staining at apical membrane (red). *D.* Crypt base model depicting the measurement of Dvl2-EGFP intensity two pixels interior to the leading (toward crypt mouth) and trailing (toward crypt base) plasma membrane of CBCs. Blue

arrows, direction of cell migration. Brackets indicate sites of measurement on the supranuclear plasma membrane. CBC, crypt-base columnar cell. Paneth, Paneth cell. *E*. Cumulative data showing the average Dvl2-EGFP intensity ratio within 1.15 µm of the supranuclear leading and trailing plasma membranes of individual mice (small circles) and overall average (large circles) for WT/Dvl2-EGFP/Rosa$^{mT/mG}$ (WT) and Cftr KO/Dvl2-EGFP/Rosa$^{mT/mG}$ (Cftr KO) sex-matched, littermate mouse pairs (n= 7 and 6 mice, respectively). Dashed line, indicates the average Dvl2-EGFP pixel intensity for the entire supranuclear region of CBC which has been set to 1.0 (Ave. intensity = 59.5±8.8 for WT and 88.5±15.9 for Cftr KO, ns, n = 7-6 mice, respectively (average of 1-3 CBCs/crypt from 2-4 crypts of passage 1 and 2 enteroids). +$p<0.002$ vs leading cell membrane. *$p<0.001$ vs. WT trailing membrane.

Measurement of Dvl2-EGFP proximity to the cell membrane was limited to the supranuclear region, i.e., between the apical pole of the nucleus and the apical membrane, due to the close apposition of the nucleus and nuclear membrane to the plasma membrane in the basal portion of the cell. To first evaluate whether pH_i in CBC cells was uniform and extended to the supranuclear region of the cell, SNARF-5F pH confocal microfluorimetry measured pH_i at the basal and apical portion of non-granulated CBC cells, serving as proxy for Lgr5+ ISCs[30]. High resolution single plane pH_i measurements were taken at the apical and basal portions of CBCs. As shown in Fig. 4B, Cftr KO enteroids exhibited a significantly more alkaline pH_i in both the apical and basal cell regions of CBCs as compared to WT, therefore confirming pH_i differences in the supranuclear region. Next, immunofluorescence studies evaluated the plasma membrane localization of the primary Wnt receptor for canonical Wnt/β-catenin signaling in ISC, i.e., Frizzled 7 (Fz7)[63]. As shown in Fig. 4C, the distribution of Fz7 appeared uniform along the entire basolateral plasma membrane of CBC cells in both WT and Cftr KO enteroids, whereas Fz7 was not localized to the apical (lumen-facing) membrane of CBCs. These studies validated investigation of Dvl2-EGFP membrane association in the supranuclear region of live CBCs.

To quantitate membrane proximity of Dvl2-EGFP to the supranuclear plasma membrane, EGFP intensity was measured within a two-pixel distance (1.15 μm) interior to the mTomato plasma membrane from the apical pole of the nucleus to the apical membrane. As depicted in Fig. 4D, two measurements were made for each CBC: one at the leading plasma membrane (most distant from the crypt base, i.e., toward crypt mouth) and the second from the trailing plasma membrane (closest to the crypt base). Differences in EGFP intensity between cells was normalized using the ratio of the average juxtamembrane EGFP intensity divided by the average EGFP intensity of all pixels in the supranuclear region of the CBC. By this analysis, the leading cell membrane in WT CBCs exhibited significantly greater juxtamembrane Dvl2-EGFP intensity than at the trailing cell membrane (see Fig. 4E). However, juxtamembrane Dvl2-EGFP intensity at the trailing cell membrane was not different from the average EGFP intensity of all supranuclear pixels, i.e., no detectable association. In contrast, the juxtamembrane Dvl2-EGFP intensity in the Cftr KO CBCs was similar to that of WT

at the leading cell membrane and significantly greater than WT at the trailing cell membrane, suggestive of a more generalized distribution of Dvl2 at the plasma membrane in Cftr KO CBCs.

The Dvl2-EGFP intensity ratio shown in Fig. 4E are averages of WT and Cftr KO sex-matched littermate mice. In analyzing our data, we found Dvl2-EGFP intensity ratio between individual crypts (consisting of the average of 1-3 CBCs/crypt) exhibited greater variability than between individual mice of the same genotype (see Supplemental Fig. 2A). However, the averages of Dvl2-EGFP intensity ratio at the leading and trailing plasma membrane of WT and Cftr KO crypts was nearly identical to the mouse averages as shown Fig. 4E. Thus, enteroid crypt averages from paired WT-Cftr KO mice also provide a robust comparison of the juxtamembrane Dvl2-EGFP intensity ratio between the two genotypes.

Neutralization of plasma membrane charge in Cftr KO enteroids reduces Dvl2 proximity to the plasma membrane. The DEP domain of Dvl binds to acidic lipid headgroups of phosphatidic acid and phosphotidlylglycerol at physiological pH[26]. In HEK293T cells, neutralization of negatively-charged phospholipids with the cationic lipid sphingosine reduced Dvl-Fz interaction by interfering with the electrostatic interaction of the Dvl DEP domain with the inner leaflet of the plasma membrane[26]. To examine the effect of neutralizing the negatively-charged inner leaflet phospholipids in Cftr KO CBCs, Dvl2-EGFP intensity at the supranuclear plasma membrane was measured in Cftr KO enteroids treated for 1 hour with 75μM sphingosine or vehicle (Fig. 5A, left). As shown in Fig 5A, right, Dvl2-EGFP intensity at both leading and trailing CBC membranes was significantly reduced in sphingosine-treated enteroids as compared to vehicle control. A comparison of enteroid crypt averages for vehicle and sphingosine treatments yielded similar results (Supplemental Fig. 2B). Thus, Dvl2 association with the plasma membrane is charge-dependent in Cftr KO crypt base epithelial cells.

Reduction of pH_i in Cftr KO enteroid CBCs reduces Dvl2 plasma membrane association. Alkalinity reduces proton interaction with the negatively-charged domains of membrane phospholipids allowing for greater interaction with Dvl2 DEP domain[26, 64]. Therefore, the pH_i in Cftr KO enteroid crypts was reduced by culturing Cftr KO/Dvl2-EGFP/Rosa$^{mT/mG}$

Figure 5

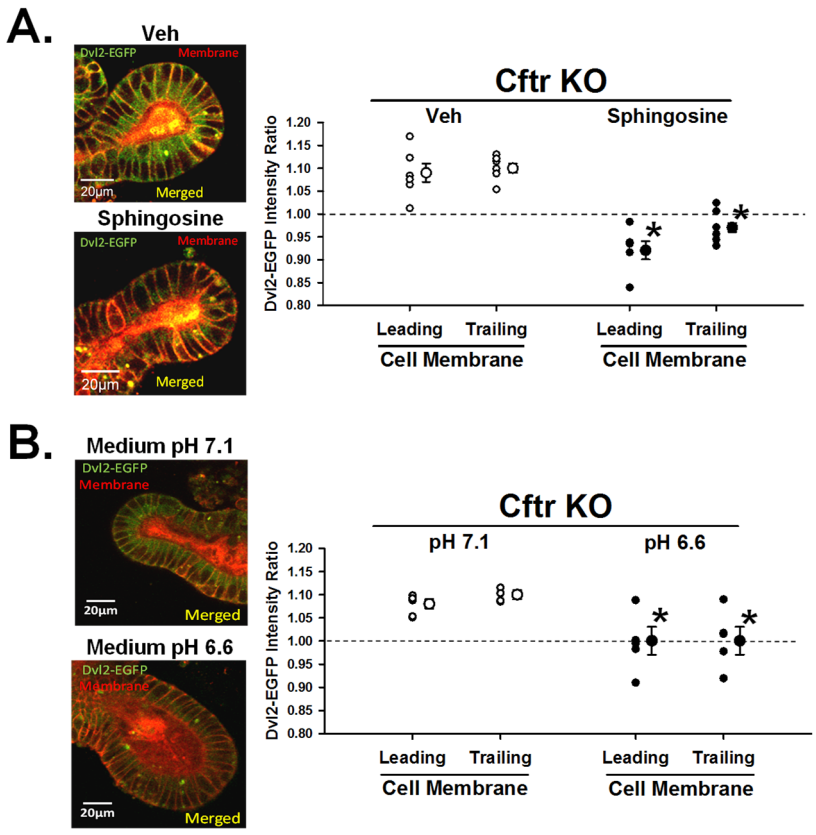

Fig. 5. *Dvl2-EGFP proximity to the plasma membrane is charge- and pH_i –dependent in Cftr KO crypt-base columnar cells.* *A.* Left, Vehicle (DMSO, top) and Sphingosine (75μM, 1hr, bottom) treated Cftr KO enteroids. Magnification, 600X. Right, cumulative data showing the average Dvl2-EGFP intensity ratio within 1.15 μm of the supranuclear leading and trailing plasma membranes of individual mice (small circles) and overall average (large circles) for WT/Dvl2-EGFP/$Rosa^{mT/mG}$ (WT) and Cftr KO/Dvl2-EGFP/$Rosa^{mT/mG}$ (Cftr KO) sex-matched, littermate mouse pairs (n= 6). Dashed line, indicates the average Dvl2-EGFP pixel intensity for the entire supranuclear region of CBC which has been set to 1.0. *p<0.001 vs. WT. Averaged data for each mouse represents measurements from 1-3 CBCs/crypt from 2-4 crypts from passage 1 and 2 etneroids. *B.* Left, Cftr KO enteroids cultured for 48 hr. in Medium pH 7.1 (top) and Medium pH 6.6 (bottom). Magnification, 600X. Right, cumulative data showing the average Dvl2-EGFP intensity ratio within 1.15 μm of the supranuclear leading and trailing plasma membranes of individual mice (small circles) and overall average (large circles) for WT/Dvl2-EGFP/$Rosa^{mT/mG}$ (WT) and Cftr KO/Dvl2-EGFP/$Rosa^{mT/mG}$ (Cftr KO) sex-matched, littermate mouse pairs (n=4). Dashed line, indicates the average Dvl2-EGFP pixel intensity for the entire supranuclear region of CBC which has been set to 1.0. *p<0.03 vs. WT. Averaged data for each mouse represents measurements from 1-3 CBCs/crypt from 2-4 crypt from passage 1 and 2 enteroids.

enteroids for 3 days in growth medium (pH 7.1) followed by 2 days in growth medium at either pH 7.1 or 6.6 (reduced [HCO_3^-], see Methods). The pH_i was reduced by -0.31 ± 0.06 in the pH 6.6 medium relative to pH 7.1 medium ($p<0.0002$, n= 13 CBC from 2-4 enteroids from 3 sex-matched WT and Cftr KO littermate mice). Overt cell and enteroid morphology were not affected by pH 6.6 medium (Fig. 5B, left). Cftr KO enteroids cultured in pH 6.6 medium, as compared to those in pH 7.1 medium, exhibited reduced Dvl2-EGFP intensity at both the leading and trailing cell plasma membranes of CBCs (Fig. 5B, right). Similar results were yielded by comparison of crypt averages for the two conditions (Supplemental Fig. 2C). Measurements of Cftr KO enteroids exposed to the pH 6.6 medium showed a significantly reduced active β-catenin as compared to pH 7.1 medium (as % of pH 7.1 (100%): pH 6.6 = 64.9±5.1%, $P<0.03$, enteroids from n=5 Cftr KO mice). Acidic conditions influences cell proliferation several ways[65]; therefore, proliferation of Cftr KO enteroids maintained in pH 6.6 medium was not investigated.

Pharmacological manipulation of Dvl2-EGFP plasma membrane association in CBCs. Recent studies have shown that the alkaline pH_i of crypt epithelium in Cftr KO enteroids can be acutely reduced by pharmacological reduction of intracellular [Cl^-] ($[Cl^-]_i$) which facilitates basolateral anion exchanger 2 normalization of pH_i [20]. To further assess the relationship between pH_i and Dvl2-EGFP membrane association, Cftr KO/Dvl2-EGFP/$Rosa^{mT/mG}$ enteroids were treated for 30 min with a sequential combination of 10 μM bumetanide (15 min), to inhibit Cl^- uptake by the $Na^+/K^+/2Cl^-$ cotransporter NKCC1, followed by 100 μM carbachol (15 min), to induce epithelial Cl^- secretion by Ca^{2+}-activated Cl^- channels (e.g., Ano1). As shown in Fig. 6A, the pharmacological treatment to normalize pH_i by reducing $[Cl^-]_i$ significantly reduced Dvl2-EGFP association at the leading and trailing cell plasma membranes in Cftr KO CBCs. In a converse experiment, WT enteroids were treated with a combination of 10 μM $Cftr_{inh}$-172 and 20 μM GlyH-101 for 1 hr. to inhibit Cftr Cl^- and HCO_3^- conductance at both extra- and intracellular sites, respectively [66]. As shown in Fig. 6B, pharmacological inhibition of Cftr to increase WT ISC pH_i (Fig. 3C) significantly increased Dvl2-EGFP association with the leading and trailing cell plasma membranes to a level similar to Cftr KO CBCs (see Fig. 4E). Both studies were paralleled by crypt averages for the two experiments (Supplemental Figure 2D and 2E).

Figure 6

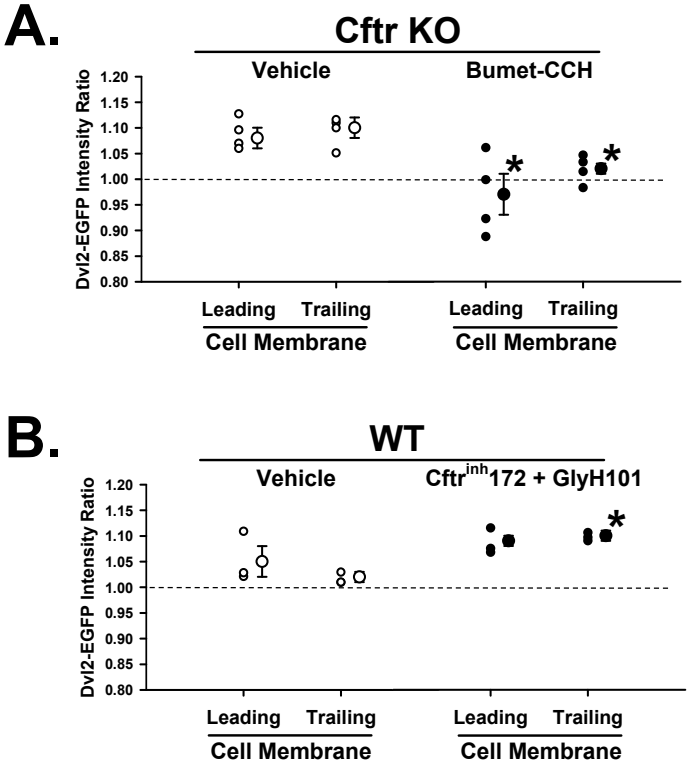

Figure 6. Pharmacological manipulation of Dvl2-EGFP plasma membrane association. *A*. Cumulative data showing the average Dvl2-EGFP intensity ratio within 1.15 µm of the supranuclear leading and trailing plasma membranes of CBCs from individual mice (small circles) and overall average (large circles). Cftr KO/Dvl2-EGFP/Rosa$^{mT/mG}$ (Cftr KO) mice were treated with Vehicle (ETOH) or sequential exposure to 50 µM bumetanide (Bumet, 15 min) followed by 100 µM carbachol (CCH, 15 min), n= 4 mice. Averaged data for each mouse represents measurements from 1-3 CBCs/crypt from 2-4 crypts from passage 1 and 2 enteroids. Dashed line, indicates the average Dvl2-EGFP pixel intensity for the entire supranuclear region of CBC which has been set to 1.0. *p<0.03 vs. Vehicle. *B*. Cumulative data showing the average Dvl2-EGFP intensity ratio within 1.15 µm of the supranuclear leading and trailing plasma membranes of individual mice (small circles) and overall average (large circles). WT/Dvl2-EGFP/Rosa$^{mT/mG}$ (WT) mice were treated with Vehicle (DMSO) or 10 µM Cftr$_{inh}$-172 plus 20 µM GlyH-101 for 1 hr. n= 3 mice. Averaged data for each mouse represents measurements from 1-3 CBCs/crypt from 2-4 crypts from passage 1 and 2 enteroids. Dashed line, indicates the average Dvl2-EGFP pixel intensity for the entire supranuclear region of CBC which has been set to 1.0. *p<0.0005 vs. Vehicle.

Discussion

Increased proliferation of the stem cell compartment is a potential risk factor for intestinal cancer[15]. Approximately three mutations occur with every division of a normal stem cell, therefore augmented stem cell proliferation raises the potential for a DNA replication error leading to a 'driver' cancer mutation[16]. Cancer genome sequencing and epidemiological studies suggest that stochastic DNA replication errors are responsible for two-thirds of the mutations in human cancers[15, 16]. One of the less commonly recognized manifestations of cystic fibrosis intestinal disease is an increased risk for gastrointestinal cancer. Surprising for a relatively young population, previous studies have shown that CF patients have a 6-10 fold increased risk for GI cancer, whereas the risk of non-digestive tract cancers in CF patients is similar to the general population[9, 67]. The risk of GI cancer increases to 20-fold in patients 20-29 years of age and includes a significantly greater number of small intestinal tumors than in the non-CF population. In accordance with increased GI cancer risk in CF patients, a recent study provided evidence that CFTR is a tumor suppressor gene in human intestinal cancer[13]. This study also demonstrated a strong propensity of CF mice for spontaneous development of intestinal tumors when aged to 1 year with a penetrance of 60% as compared to 0% in WT mice. The majority of tumors in CF mice were in the small intestine. Together with increased ISC proliferation, the CF small intestinal environment presents additional cancer risk factors including low-grade inflammation[4, 5, 11], small bowel bacterial overgrowth[3, 12], dysbiosis[68-70] and goblet cell metaplasia[71]. With advances in CF respiratory therapy leading to increased life expectancy and the current prevalence of lung transplantation in CF patients[8], there is a need to better understand the causes of intestinal hyperproliferation in the adult CF intestine and its relationship with cancer incidence.

Increased ISC proliferation in the Cftr KO intestine was maintained in early passage primary organoid culture, suggestive of an inherent epithelial phenotype. The Cftr KO proliferative phenotype was apparent through culture passages 1 and 2, but proliferation rates of WT and Cftr KO enteroid crypts converged by passage 4. However, matched WT enteroids at passage 4 assumed a CF phenotype with decreased Cftr expression

and increased proliferation, ostensibly due to selection against slower growth by cells (ISCs) expressing Cftr[43, 44]. In vivo, the CF intestinal environment may promote epithelial proliferation through disease factors known to increase the risk for GI cancer. One factor is intestinal inflammation; however, studies of small intestinal inflammation in both CF patients and CF mice indicate a relatively mild presentation. Neutrophil and mononuclear cell infiltration of the submucosa are moderate without overt mucosal damage[5, 11]. Gene expression studies indicate immune activation in the small intestine of CF patients[4, 5]. In CF mice, changes in innate immunity genes were also noted but minimized by therapeutic intervention to prevent bowel obstruction by maintaining the mice on a polyethylene glycol (PEG) osmotic laxative in the drinking water[72]. CF mice in the present investigation and in the study by Than et al. that showed a high incidence of GI tumors were maintained on the PEG laxative, which may reduce the contribution of inflammation-induced genetic/epigenetic changes. Together with evidence that Cftr is expressed and functional in murine Lgr5+ ISC, we tentatively conclude that hyperproliferation in the CF intestine is a consequence of losing the growth suppressive function of Cftr. However, without further investigation, it is difficult to eliminate the possibility that growth stimulation in the Cftr KO enteroids includes epigenetic changes secondary to the CF intestinal environment that are carried into culture.

Wnt/β-catenin signaling is required for proliferation and maintenance of small intestinal stem cells[28]. We found that Wnt/β-catenin signaling, as indicated by active β-catenin and down-stream Lef1 protein amounts, is increased in both freshly isolated crypts and early passage enteroids of Cftr KO mice. This finding is consistent with higher numbers of Lgr5+ stem cells in the intestine/enteroids of Cftr KO/Lgr5-EGFP mice. Further studies revealed Cftr protein expression in sorted $SOX9^{EGFPLo}$ cells, an alkaline pH_i in Lgr5+-EGFP ISCs in the absence of Cftr activity and greater proliferation in ISC-enriched enterospheres from Cftr KO mice, as compared to WT. This evidence supports previous studies identifying CFTR as a down-stream target for the terminal effector of Wnt/β-catenin signaling, i.e., T cell factor 4, and suggests that Cftr may play a role in maintaining the balance between intestinal proliferation and differentiation[49]. As a direct target gene, Cftr may modulate ISC proliferation through actions on the cell

cycle. In T and B lymphocytes cell lines, it has been shown that a CFTR-dependent Cl^- permeability is increased during the G1 phase of the cell cycle which could be augmented by increasing intracellular cAMP[73]. This coordinates nicely with evidence in other cell types that increased cAMP and reduced intracellular [Cl^-] during G1 leads to cell cycle arrest by a p21-dependent mechanism[74, 75]. However, potential involvement of Cftr as a growth suppressant in ISC by cell cycle regulation does not elucidate the pathway of increased Wnt/β-catenin signaling in the crypts of the Cftr KO intestine.

The pathogenesis connecting dysregulated Wnt/β-catenin signaling to the absence of an apical membrane anion channel is unlikely to be direct. Although previous studies have shown CFTR to interact with several proteins thereby affecting various cell processes[76, 77], the undisputed function of CFTR is to provide epithelial Cl^- and HCO_3^- permeability. Loss of this permeability in CF disease has been associated with dehydration and reduced pH of the airway and intestinal surfaces, increased mucus viscosity, and deficits of innate immunity[78-83]. Another cellular consequence of CFTR loss is dysregulation of pH_i in the alkaline range, which was recently shown to be dependent on the combined intracellular retention of Cl^- and HCO_3^- [20]. Alkaline pH_i is conducive to cell proliferation by positive effects on cell cycle transitions and DNA replication[21, 22], but is known to facilitate Wnt signaling by increasing the interaction of Dvl with the inner plasma membrane to stabilize binding with the Wnt receptor, Fz[26]. Dvl possesses a polycationic motif that targets the protein to the negatively charged inner leaflet, similar to the process used for subcellular localization of a variety of polycationic proteins including K-Ras and proteins associated with endosomes (which demonstrate defective recycling in CF cells[84]). Discovered through a genome-wide RNAi screen of *Drosphila* cells, Dsh membrane localization required Na^+/H^+ exchanger 2 activity to reduce intracellular [H^+] and improve Fz recruitment of Dsh[26]. Although serial replacement of basic DEP residues indicated that membrane stabilization of Dsh was more important to non-canonical PCP Wnt signaling than canonical Wnt/β-catenin signaling, it is reasonable that Dvl membrane stabilization by an alkaline pH_i in CF cells should also facilitate canonical Wnt/β-catenin signaling. Live imaging of enteroids from WT/ or Cftr KO/Dvl2 KO/Dvl2-EGFP/$Rosa^{mT/mG}$ mice supported this hypothesis by

showing greater juxtamembrane association of Dvl in Cftr KO CBC cells. Dvl membrane association was both charge- and pH_i-dependent and could be predictably manipulated by pharmacological treatments to reduce intracellular [Cl^-] in Cftr KO cells or inhibit Cftr in WT cells. An unexpected outcome in studies of WT CBCs was increased Dvl membrane association at the leading cell membrane (relative to migration from the crypt base). Although not investigated, it is tempting to speculate that the leading cell membrane may generate a localized pH_i gradient that not only increases Dvl localization but also facilitates cell migration, as has been shown in migrating fibroblasts[85]. The demonstration of greater Dvl association with the plasma membrane in Cftr KO CBCs in situ is consistent with our hypothesis, but does not directly establish increased Fz-Dvl interaction. Quantitative information regarding the amplification of signal through the cascade of the Wnt/β-catenin pathway and discrete genetic manipulations of an appropriate cell line will be needed to estimate the contribution of Dvl membrane stabilization to increased Wnt/β-catenin signaling.

Another inference of increased Dvl association with the supranuclear plasma membrane in Cftr KO crypt epithelium is facilitation of non-canonical Wnt pathways of planar cell polarity (PCP) and directional cell movement[86, 87]. Increased cell migration from the crypts as a consequence of increased epithelial proliferation has been shown in the Cftr KO mouse in vivo[14]. In intestinal crypts, cell migration must be closely coordinated with proliferation and involves remodeling of the adherens junctions by processes that are not well-understood in this context[88]. Disheveled is a crucial component of the PCP pathway as previously shown for polarized cell migration of mouse embryonic fibroblasts[89]. Disheveled transduces signals from Wnt-liganded Fz and the co-receptor Ror2, a tyrosine kinase-like orphan receptor, which directs c Jun N-terminal kinase (JNK) for activation of c-Jun, resulting in cytoskeletal reorganization and polarized cell migration[27]. Studies in Xenopus show that polarization of ectodermal cells involves xDsh accumulation with Fz7 at the apical adherens junctions in response to Wnt11[90]. Disheveled may also provide a link between the Fz/Ror2 pathway and Cdc42 for polarized cell migration. The Rho family GTPase Cdc42 is a major determinant of apical-basal polarity in intestinal epithelium[91]. Cdc42 is recruited by guanine exchange factors, a process facilitated by an alkaline pH_i,[92] and can bind partitioning complex

members Par3 and Par6 at the tight junctional complex and apical membrane, respectively[93]. This process leads to activation of an atypical protein kinase C (aPKC, PKCζ), potentially regulated by the DEP domain of Dvl[27], which facilitates polarized cell migration[94].

In conclusion, our data demonstrate that the absence of Cftr activity in murine ISC establishes in an alkaline pH_i that potentially facilitates canonical Wnt/β-catenin signaling by increasing the stability of the Wnt transducer Dvl at the plasma membrane. The rate of ISC proliferation and changes of signaling in the Cftr KO intestine are moderate, but over the course of a lifetime create an insidious process that raises the risk of intestinal carcinogenesis. When placed within the context of the Cftr KO intestinal environment, with attendant inflammation and dysbiosis, a significant risk for neoplastic development would be predicted which is consistent with the high tumor penetrance (~60%) exhibited by aged CF mice[13]. However, to best of our knowledge, epithelial proliferation rates and Wnt/β-catenin signaling of the intestine have not been evaluated in CF patients. These data from the Cftr KO mouse model should illuminate the need to investigate this potential risk factor in CF. With continued improvements in care and an aging CF population, the incidence of digestive tract cancer will likely increase without more attention to clinical screening of CF patients for GI cancer and investigations identifying the underlying processes by which life-long dysfunction of an epithelial anion channel yields increased gastrointestinal cancer risk.

Acknowledgements

The authors would like to acknowledge the assistance of the Dalton Cardiovascular Research Center Live Cell Imaging Core and Dr. Luis Martinez-Lemus (director). Authors also thank the National Institutes of Health for ImageJ software. The research was supported by a grant from the National Institute of Diabetes and Digestive and Kidney Disease (LLC: NIDDK 5R01DK048816) and the Cystic Fibrosis Foundation (LLC: CLARKE11G0; CLAEKE15G0; JL: LIU13Q10).

References

1. Anderson MP, Gregory RJ, Thompson S, et al. Demonstration that CFTR is a chloride channel by alteration of its anion selectivity. Science 1991;253:202-205.
2. Poulsen JH, Fischer H, Illek B, et al. Bicarbonate conductance and pH regulatory capability of cystic fibrosis transmembrane conductance regulator. Proceedings of the National Academy of Sciences 1994;91:5340-5344.
3. Norkina O, Burnett TG, De Lisle RC. Bacterial overgrowth in the cystic fibrosis transmembrane conductance regulator null mouse small intestine. Infect Immun 2004;72:6040-6049.
4. Smyth RL, Croft NM, O'Hea U, et al. Intestinal inflammation in cystic fibrosis. Arch Dis Child 2000;82:394-399.
5. Raia V, Maiuri L, De Ritis G, et al. Evidence of chronic inflammation in morphologically normal small intestine of cystic fibrosis patients. Pediatr Res 2000;47:344-350.
6. Welsh MJ, Tsui LC, Boat TF, et al. Cystic Fibrosis. In: Scriver CR, Beaudet AL, Sly WS, Valle D, Fredrickson DS, eds. Metabolic and Molecular Basis of Inherited Disease. Volume 7th. New York: McGraw Hill, 1995:3799-3863.
7. Borowitz D, Durie PR, Clarke LL, et al. Gastrointestinal outcomes and confounders in cystic fibrosis. J Pediatr Gastroenterol Nutr 2005;41:273-285.
8. Maisonneuve P, Fitzsimmons SC, Neglia JP, et al. Cancer risk in nontransplanted and transplanted cystic fibrosis patients: A 10-year study. J.Natl.Cancer Inst. 2003;95:381-387.
9. Neglia JP, Fitzsimmons SC, Maisonneuve P, et al. The risk of cancer among patients with cystic fibrosis. N.Engl.J.Med. 1995;332:494-499.
10. Snouwaert JN, Brigman KK, Latour AM, et al. An animal model for cystic fibrosis made by gene targeting. Science 1992;257:1083-1088.
11. Norkina O, Kaur S, Ziemer D, et al. Inflammation of the cystic fibrosis mouse small intestine. Am J Physiol-Gastrointest Liver Physiol 2004;286:G1032-41.
12. Clarke LL, Gawenis LR, Bradford EM, et al. Abnormal Paneth cell granule dissolution and compromised resistance to bacterial colonization in the intestine of CF mice. Am J Physiol-Gastrointest Liver Physiol 2004;286:G1050-G1058.
13. Than BLN, Linnekamp JF, Starr TK, et al. CFTR is a tumor suppressor gene in murine and human intestinal cancer. Oncogene 2016.
14. Gallagher AM, Gottlieb RA. Proliferation, not apoptosis, alters epithelial cell migration in small intestine of CFTR null mice. Am J Physiol-Gastr L 2001;281:G681-G687.
15. Tomasetti C, Vogelstein B. Variation in cancer risk among tissues can be explained by the number of stem cell divisions. Science 2015;347:78-81.
16. Tomasetti C, Li L, Vogelstein B. Stem cell divisions, somatic mutations, cancer etiology, and cancer prevention. Science 2017;355:1330-1334.
17. Strong TV, Boehm K, Collins FS. Localization of cystic fibrosis transmembrane conductance regulator mRNA in the human gastrointestinal tract by in situ hybridization. J.Clin.Invest. 1994;93:347-354.
18. Ameen NA, Alexis J, Salas P. Cellular localization of the cystic fibrosis transmembrane conductance regulator in mouse intestinal tract. Histochem Cell Biol 2000;114:69-75.
19. Liu J, Walker NM, Cook MT, et al. Functional Cftr in crypt epithelium of organotypic enteroid cultures from murine small intestine. Am J Physiol-Cell Physiol 2012;302:C1492-C1503.
20. Walker NM, Liu J, Stein SR, et al. Cellular chloride and bicarbonate retention alters intracellular pH regulation in Cftr KO crypt epithelium. American Journal of Physiology - Gastrointestinal and Liver Physiology 2016;310:G70-G80.

21. Putney LK, Barber DL. Na-H exchange-dependent increase in intracellular pH times G 2 /M entry and transition. J Biol Chem 2003;278:44645-44649.
22. Schreiber R. Ca2+ signaling, intracellular pH and cell volume in cell proliferation. J.Memb.Biol. 2005;205:129-137.
23. Casey JR, Grinstein S, Orlowski J. Sensors and regulators of intracellular pH. Nat Rev Mol Cell Biol 2010;11:50-61.
24. Webb BA, Chimenti M, Jacobson MP, et al. Dysregulated pH: a perfect storm for cancer progression. Nat Rev Cancer 2011;11:671-7.
25. Young BP, Shin JJH, Orij R, et al. Phosphatidic Acid Is a pH Biosensor That Links Membrane Biogenesis to Metabolism. Science 2010;329:1085-1088.
26. Simons M, Gault WJ, Gotthardt D, et al. Electrochemical cues regulate assembly of the Frizzled/Dishevelled complex at the plasma membrane during planar epithelial polarization. Nature Cell Biol. 2009;11:286-294.
27. Gao C, Chen YG. Dishevelled: the hub of Wnt signaling. Cell Signal 2010;22:717-727.
28. Fevr T, Robine S, Louvard D, et al. Wnt/beta-catenin is essential for intestinal homeostasis and maintenance of intestinal stem cells. Molecular and Cellular Biology 2007;27:7551-7559.
29. De Lisle RC, Mueller R, Boyd M. Impaired Mucosal Barrier Function in the Small Intestine of the Cystic Fibrosis Mouse. Journal of Pediatric Gastroenterology and Nutrition 2011;53:371-379.
30. Sato T, Vries RG, Snippert HJ, et al. Single Lgr5 stem cells build crypt-villus structures in vitro without a mesenchymal niche. Nature 2009;459:262-265.
31. Lee Y-N, Gao Y, Wang H-y. Differential mediation of the Wnt canonical pathway by mammalian Dishevelleds-1, -2, and -3. Cell Signal 2008;20:443-452.
32. Etheridge SL, Ray S, Li S, et al. Murine Dishevelled 3 Functions in Redundant Pathways with Dishevelled 1 and 2 in Normal Cardiac Outflow Tract, Cochlea, and Neural Tube Development. PLoS Genet 2008;4:e1000259.
33. Clarke LL, Gawenis LR, Franklin CL, et al. Increased survival of CFTR knockout mice using an oral osmotic laxative. Lab Animal Sci 1996;46:612-618.
34. Wang J, Hamblet NS, Mark S, et al. Dishevelled genes mediate a conserved mammalian PCP pathway to regulate convergent extension during neurulation. Development 2006;133:1767-1778.
35. Liu J, Lu W, Guha S, et al. Cystic fibrosis transmembrane conductance regulator (CFTR) contributes to reacidification of alkalinized lysosomes in RPE cells. Am J Physiol-Cell Physiol 2012;303:C160-C169.
36. Livak KJ, Schmittgen TD. Analysis of relative gene expression data using real-time quantitative PCR and the 2(-Delta Delta C(T)) Method. Methods 2001;25:402-8.
37. Formeister EJ, Sionas AL, Lorance DK, et al. Distinct SOX9 levels differentially mark stem/progenitor populations and enteroendocrine cells of the small intestine epithelium. Am J Physiol-Gastr L 2009;296:G1108-G1118.
38. Simpson JE, Gawenis LR, Walker NM, et al. Chloride conductance of CFTR facilitates basal Cl^-/HCO_3^- exchange in the villous epithelium of intact murine duodenum. Am J Physiol-Gastrointest Liver Physiol 2005;288:G1241-G1251.
39. Ootani A, Li X, Sangiorgi E, et al. Sustained in vitro intestinal epithelial culture within a Wnt-dependent stem cell niche. Nat Med 2009;15:701-706.
40. Barker N, Van Es JH, Kuipers J, et al. Identification of stem cells in small intestine and colon by marker gene Lgr5. Nature 2007;449:1003-1008.
41. Karrasch T, Spaeth T, Allard B, et al. PI3K-dependent GSK3s(Ser9)-phosphorylation is implicated in the intestinal epithelial cell wound-healing response. PLoS ONE [Electronic Resource] 2011;6:e26340.

42. Diks SH, Hardwick JC, Diab RM, et al. Activation of the Canonical β-Catenin Pathway by Histamine. Journal of Biological Chemistry 2003;278:52491-52496.
43. Clarke LL, Gawenis LR, Hwang TC, et al. A domain mimic increases DF508 CFTR trafficking and restores cAMP-stimulated anion secretion in cystic fibrosis epithelia. Am J Physiol-Cell Ph 2004;287:C192-C199.
44. Schiavi SC, Abdelkader N, Reber S, et al. Biosynthetic and growth abnormalities are associated with high-level expression of CFTR in heterologous cells. Am J Physiol-Cell Ph 1996;270:C341-C351.
45. van Noort M, Meeldijk J, van der Zee R, et al. Wnt Signaling Controls the Phosphorylation Status of β-Catenin. Journal of Biological Chemistry 2002;277:17901-17905.
46. van der Flier LG, Sabates-Bellver J, Oving I, et al. The intestinal Wnt/TCF signature. Gastroenterology 2007;132:628-632.
47. Fre S, Pallavi SK, Huyghe M, et al. Notch and Wnt signals cooperatively control cell proliferation and tumorigenesis in the intestine. Proceedings of the National Academy of Sciences 2009;106:6309-6314.
48. VanDussen KL, Carulli AJ, Keeley TM, et al. Notch signaling modulates proliferation and differentiation of intestinal crypt base columnar stem cells. Development 2012;139:488-497.
49. Paul T, Li S, Khurana S, et al. The epigenetic signature of CFTR expression is co-ordinated via chromatin acetylation through a complex intronic element. Biochem J 2007;408:317-326.
50. Gracz AD, Ramalingam S, Magness ST. Sox9 expression marks a subset of CD24-expressing small intestine epithelial stem cells that form organoids in vitro. Am J Physiol-Gastr L 2010;298:G590-G600.
51. Hirokawa M, Takeuchi T, Chu S, et al. Cystic fibrosis gene mutation reduces epithelial cell acidification and injury in acid-perfused mouse duodenum. Gastroenterology 2004;127:1162-1173.
52. Elgavish A. High intracellular pH in CFPAC: a pancreas cell line from a patient with cystic fibrosis is lowered by retrovirus-mediated CFTR gene transfer. Biochem Bioph Res Co 1991;180:342-348.
53. Stelzner M, Helmrath M, Dunn JCY, et al. A nomenclature for intestinal in vitro cultures. Am J Physiol-Gastr L 2012;302:G1359-G1363.
54. VAnDussen KL, Marinshaw, J.M., Miyoshi, H., Ciorba, M.A., Stappenbeck, T.S. Efficient Isolation, Expansion and Differentiation of Human Epithelial Stem Cells From Endoscopic Biopsies of the Gastrointestinal Tract. Gastroenterology 2013;144:S-62-S-63.
55. Miyoshi H, Stappenbeck TS. In vitro expansion and genetic modification of gastrointestinal stem cells in spheroid culture. Nature Protocols 2013;8:2471-82.
56. Sato T, Stange DE, Ferrante M, et al. Long-term Expansion of Epithelial Organoids From Human Colon, Adenoma, Adenocarcinoma, and Barrett's Epithelium. Gastroenterology 2011;141:1762-1772.
57. Yin X, Farin HF, van Es JH, et al. Niche-independent high-purity cultures of Lgr5+ intestinal stem cells and their progeny. Nat Meth 2014;11:106-112.
58. Dekkers JF, Wiegerinck CL, de Jonge HR, et al. A functional CFTR assay using primary cystic fibrosis intestinal organoids. Nat Med 2013;advance online publication.
59. van der Flier LG, Haegebarth A, Stange DE, et al. OLFM4 is a robust marker for stem cells in human intestine and marks a subset of colorectal cancer cells. Gastroenterology 2009;137:15-17.
60. Sangiorgi E, Capecchi MR. Bmi1 is expressed in vivo in intestinal stem cells. Nat Genet 2008;40.
61. Grumolato L, Liu G, Mong P, et al. Canonical and noncanonical Wnts use a common mechanism to activate completely unrelated coreceptors. Gene Dev 2010;24:2517-2530.

62. Pan WJ, Pang SZ, Huang T, et al. Characterization of Function of Three Domains in Dishevelled-1: DEP Domain is Responsible for Membrane Translocation of Dishevelled-1. Cell Res 2004;14:324-330.
63. Flanagan DJ, Phesse TJ, Barker N, et al. Frizzled7 functions as a Wnt receptor in intestinal epithelial Lgr5(+) stem cells. Stem Cell Reports 2015;4:759-67.
64. Wang W, Anderson NA, Travesset A, et al. Regulation of the electric charge in phosphatidic acid domains. J Phys Chem B 2012;116:7213-20.
65. Fitzgerald RO, MB; Triadafilopoulos, G. Acid modulation of HT29 cell growth and differentiation. J Cell Sci 1997;110:663-671.
66. Liu X, Luo M, Zhang L, et al. Bioelectric Properties of Chloride Channels in Human, Pig, Ferret, and Mouse Airway Epithelia. Am J Resp Cell Mol 2007;36:313-323.
67. Gory I, Brown G, Wilson J, et al. Increased risk of colorectal neoplasia in adult patients with cystic fibrosis: a matched case-control study. Scand J Gastroenterol 2014;49:1230-6.
68. Garg M, Ooi CY. The Enigmatic Gut in Cystic Fibrosis: Linking Inflammation, Dysbiosis, and the Increased Risk of Malignancy. Current Gastroenterology Reports 2017;19:6.
69. Manor O, Levy R, Pope CE, et al. Metagenomic evidence for taxonomic dysbiosis and functional imbalance in the gastrointestinal tracts of children with cystic fibrosis. Scientific Reports 2016;6:22493.
70. Lynch SV, Goldfarb KC, Wild YK, et al. Cystic fibrosis transmembrane conductance regulator knockout mice exhibit aberrant gastrointestinal microbiota. Gut Microbes 2013;4:41-7.
71. Qazi TM, O'Brien MJ, Farraye FA, et al. Epidemiology of goblet cell and microvesicular hyperplastic polyps. American Journal of Gastroenterology 2014;109:1922-32.
72. De Lisle RC, Roach E, Jansson K. Effects of laxative and N-acetylcysteine on mucus accumulation, bacterial load, transit, and inflammation in the cystic fibrosis mouse small intestine. Am J Physiol-Gastrointest Liver Physiol 2007;293:G577-G584.
73. Bubien JK, Kirk KL, Rado TA, et al. Cell cycle dependence of chloride permeability in normal and cystic fibrosis lymphocytes. Science 1990;248:1416-1419.
74. Miyazaki H, Shiozaki A, Niisato N, et al. Chloride ions control the G1/S cell-cycle checkpoint by regulating the expression of p21 through a p53-independent pathway in human gastric cancer cells. Biochemical and Biophysical Research Communications 2008;366:506-512.
75. Zeilig CE, Goldberg ND. Cell-cycle-related changes of 3':5'-cyclic GMP levels in Novikoff hepatoma cells. Proceedings of the National Academy of Sciences of the United States of America 1977;74:1052-6.
76. Ko SBH, Zeng W, Dorwart MR, et al. Gating of CFTR by the STAS domain of SLC26 transporters. Nature Cell Biol. 2004;6:343-350.
77. Rymut SM, Harker A, Corey DA, et al. Reduced microtubule acetylation in cystic fibrosis epithelial cells. American Journal of Physiology - Lung Cellular and Molecular Physiology 2013;305:L419-L431.
78. Coakley RD, Grubb BR, Paradiso AM, et al. Abnormal surface liquid pH regulation by cultured cystic fibrosis bronchial epithelium. Proceedings of the National Academy of Sciences 2003;100:16083-16088.
79. Henderson AG, Ehre C, Button B, et al. Cystic fibrosis airway secretions exhibit mucin hyperconcentration and increased osmotic pressure. The Journal of Clinical Investigation 2014;124:3047-3060.
80. Li X, Tang XX, Vargas Buonfiglio LG, et al. Electrolyte transport properties in distal small airways from cystic fibrosis pigs with implications for host defense. American Journal of Physiology - Lung Cellular and Molecular Physiology 2016;310:L670-L679.

81. Abou Alaiwa MH, Beer AM, Pezzulo AA, et al. Neonates with cystic fibrosis have a reduced nasal liquid pH; a small pilot study. Journal of Cystic Fibrosis 2014;13:373-7.
82. Pezzulo AA, Tang XX, Hoegger MJ, et al. Reduced airway surface pH impairs bacterial killing in the porcine cystic fibrosis lung. Nature 2012;487:109-13.
83. Kaur S, Norkina O, Ziemer D, et al. Acidic duodenal pH alters gene expression in the cystic fibrosis mouse pancreas. Am J Physiol-Gastrointest Liver Physiol 2004;287:G480-90.
84. Bradbury NA, Jilling T, Berta G, et al. Regulation of plasma membrane recycling by CFTR. Science 1992;256:530-2.
85. Denker SP, Barber DL. Cell migration requires both ion translocation and cytoskeletal anchoring by the Na-H exchanger NHE1. The Journal of Cell Biology 2002;159:1087-1096.
86. Park TJ, Gray RS, Sato A, et al. Subcellular Localization and Signaling Properties of Dishevelled in Developing Vertebrate Embryos. Curr Biol 2005;15:1039-1044.
87. Novellasdemunt L, Antas P, Li VS. Targeting Wnt signaling in colorectal cancer. A Review in the Theme: Cell Signaling: Proteins, Pathways and Mechanisms. Am J Physiol Cell Physiol 2015;309:C511-21.
88. Madara J, Trier J. The functional morphology of the mucosa of the small intestine. In: Johnson L, ed. Physiology of the Gastrointestinal Tract. Volume 2. 3rd ed. New York: Raven Press, 1994:1577-1622.
89. Nishita M, Yoo SK, Nomachi A, et al. Filopodia formation mediated by receptor tyrosine kinase Ror2 is required for Wnt5a-induced cell migration. J.Cell Biol. 2006;175:555-562.
90. Yamanaka H, Nishida E. Wnt11 stimulation induces polarized accumulation of Dishevelled at apical adherens junctions through Frizzled7. Genes Cells 2007;12:961-967.
91. Melendez J, Liu M, Sampson L, et al. Cdc42 coordinates proliferation, polarity, migration, and differentiation of small intestinal epithelial cells in mice. Gastroenterology 2013;145:808-19.
92. Frantz C, Karydis A, Nalbant P, et al. Positive feedback between Cdc42 activity and H+ efflux by the Na-H exchanger NHE1 for polarity of migrating cells. J Cell Biol 2007;179:403-410.
93. Martin-Belmonte F, Gassama A, Datta A, et al. PTEN-mediated apical segregation of phosphinositides controls epithelial morphogenesis through Cdc42. Cell 2007;128:383-397.
94. Minami Y, Oishi I, Endo M, et al. Ror-family receptor tyrosine kinases in noncanonical Wnt signaling: Their implication in develomental morphogenesis and human diseases. Dev Dynam 2010;239:1-15.

Supplemental Data

Supplemental Figure 1

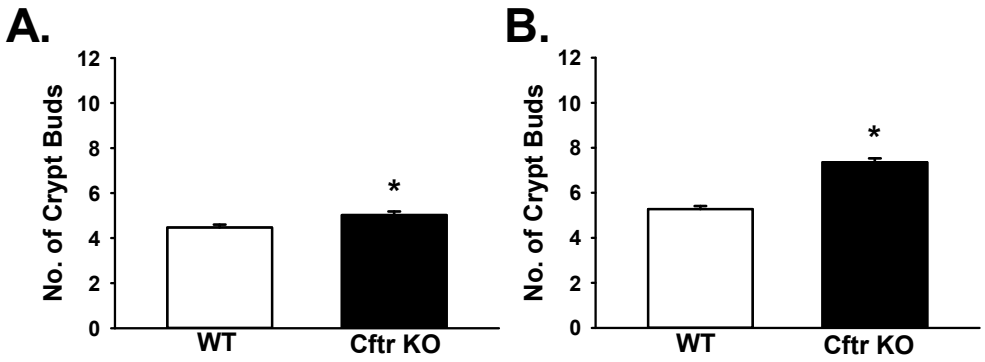

Suppl. Fig. 1. *De novo crypt formation in enteroids from sex-matched Cftr KO and WT mice*. *A*: Cumulative data of lateral crypt bud formation of WT and Cftr KO enteroids cultured for 7 days. n= 670-788 enteroids from 3 WT/Cftr KO pairs. *P<0.001. *B*: Cumulative data of lateral crypt bud formation of WT and Cftr KO enteroids with increased growth factor concentration (4X growth medium). n= 670-728 enteroids from 3 WT/Cftr KO pairs. **P*<0.001.

Supplemental Figure 2

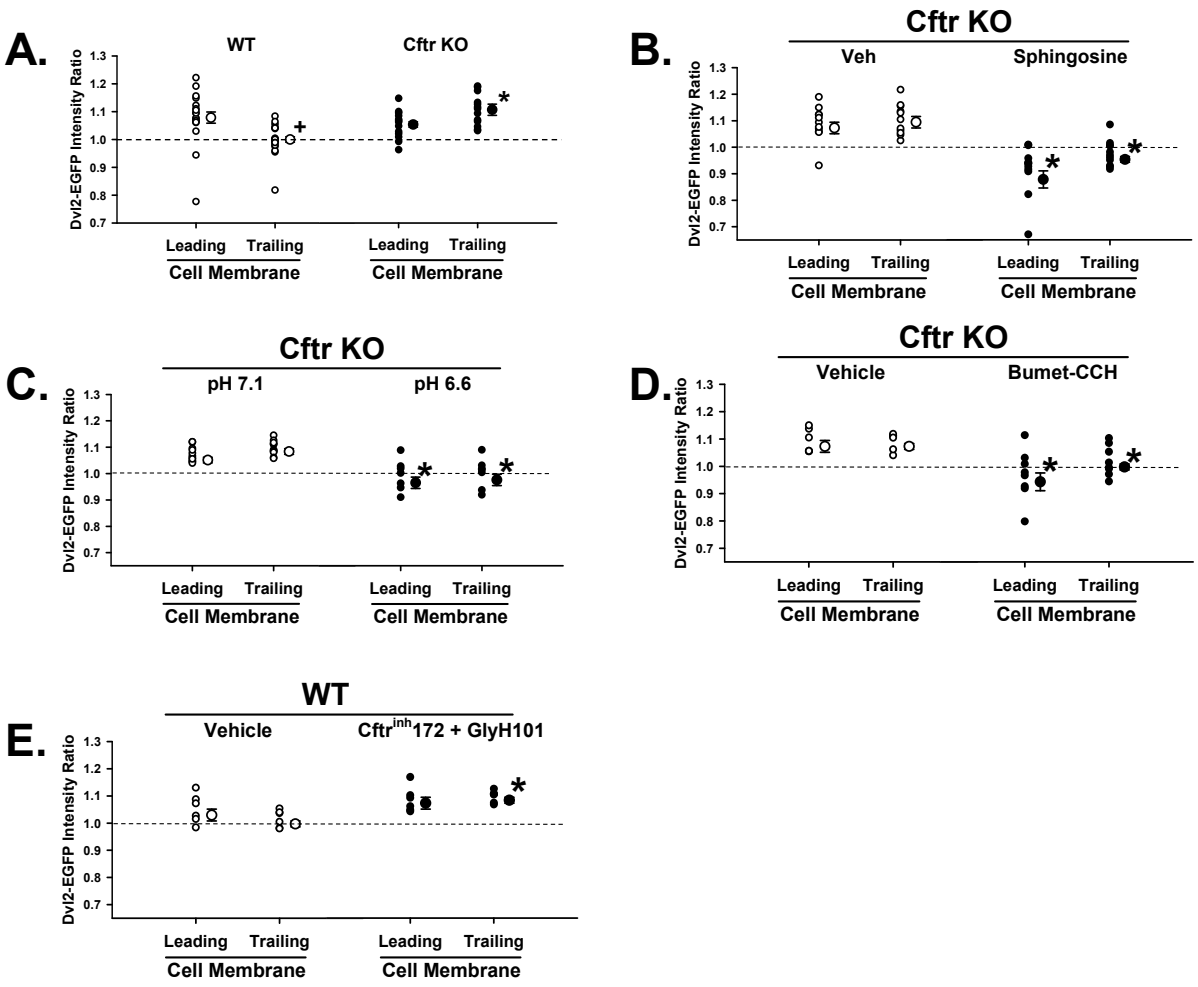

Suppl. Fig. 2. Cumulative data showing the average Dvl2-EGFP intensity ratio within 1.15 µm of the supranuclear leading and trailing plasma membranes of individual crypts (small circles) and overall crypt average (large circles). A. Comparison of WT/Dvl2-EGFP/Rosa$^{mT/mG}$ (WT, white circles) and Cftr KO/Dvl2-EGFP/Rosa$^{mT/mG}$ (Cftr KO, dark circles) sex-matched, littermate mouse pairs. Dashed line, indicates the average Dvl2-EGFP pixel intensity for the entire supranuclear region of CBC which has been set to 1.0. +p<0.0002 vs leading cell membrane. *p<0.00002 vs. WT trailing membrane. n = 7-6 mice, respectively. Average of 1-3 CBCs/crypt from 18-14 crypts of WT and Cftr KO enteroids , respectively. **B. Effect of sphingosine on Dvl2-EGFP membrane association by crypt**. Average Dvl2-EGFP

intensity ratio at supranuclear leading and trailing plasma membranes of individual crypts (small circles) and overall crypt average (large circles) for Vehicle (DMSO, Veh, white circles) and Sphingosine (75 μM, 1 hr., dark circles) treated Cftr KO/Dvl2-EGFP/Rosa$^{mT/mG}$ (Cftr KO) sex-matched littermate mice. Dashed line, indicates the average Dvl2-EGFP pixel intensity for the entire supranuclear region of CBC which has been set to 1.0. *p<0.001 vs. Veh (leading), p<0.00002 (trailing). n = 6 mice. Average of 1-3 CBCs/crypt from 11 crypts of Vehicle- and Spingosine-treated Cftr KO enteroids. **C. Effect of reduced pH medium on Dvl2-EGFP membrane association by crypt.** Average Dvl2-EGFP intensity ratio at the supranuclear leading and trailing plasma membranes of individual crypts (small circles) and overall crypt average (large circles) for pH 7.1 and pH 6.6 (48 hrs.) exposed Cftr KO/Dvl2-EGFP/Rosa$^{mT/mG}$ (Cftr KO) mice. Dashed line, indicates the average Dvl2-EGFP pixel intensity for the entire supranuclear region of CBC which has been set to 1.0. *p<0.005 vs. pH 7.1 (leading), p<0.0001 (trailing). n = 4 mice. Average of 1-3 CBCs/crypt from 11-7 crypts of pH 7.1- and pH 6.6-exposed Cftr KO enteroids , respectively. **D. Effect of pharmacological reduction of intracellular [Cl^-] (and pH_i) manipulation of Dvl2-EGFP membrane association in Cftr KO enteroid crypts.** Average Dvl2-EGFP intensity ratio at the supranuclear leading and trailing plasma membranes of individual crypts (small circles) and overall crypt average (large circles) for Vehicle (ETOH, Veh, white circles) and sequential Bumetanide (Bumet, 50 μM, 15 min) followed by Carbachol (CCH, 100 μM, 15 min, dark circles)-treated Cftr KO/Dvl2-EGFP/Rosa$^{mT/mG}$ (Cftr KO) mice. Dashed line, indicates the average Dvl2-EGFP pixel intensity for the entire supranuclear region of CBC which has been set to 1.0. *p<0.05 vs. Veh (leading), p<0.02 (trailing). n = 4 mice. Average of 1-3 CBCs/crypt from 6-8 crypts of Vehicle- and Bumet-CCH-treated Cftr KO enteroids, respectively. **E. Effect of pharmacological blockade of Cftr on Dvl2-EGFP membrane association in WT enteroid crypts.** Average Dvl2-EGFP intensity ratio at the supranuclear leading and trailing plasma membranes of individual crypts (small circles) and overall crypt average (large circles) for Vehicle- (DMSO, white circles) and combined treatment with $Cftr_{inh}$-172 (10μM) and GlyH-101 (20 μM) for 1 hr. in WT/Dvl2-EGFP/Rosa$^{mT/mG}$ (WT) mice. Dashed line, indicates the average Dvl2-EGFP pixel intensity for the entire supranuclear region of CBC which has been set to 1.0. *p<0.0004 vs. Vehicle. n = 3 mice. Average of 1-3 CBCs/crypt from 6 crypts of WT enteroids , respectively.